Coverage in One-Dimensional Wireless Networks with Infrastructure Nodes and Relay Extensions

K. P. Naveen, *Member, IEEE* and Anurag Kumar, *Fellow, IEEE*

***Abstract*—We consider a wireless network comprising two types of nodes, namely, *sinks* and *relays*. The sink nodes are connected to a wireline infrastructure, while the relay nodes are used to extend the region covered by providing multi-hop paths to the sink nodes. Restricting to the one-dimensional setting, our objective is to characterize the fraction of covered region as a function of sink and relay node densities. We first compare and contrast our *infrastructure-based* model with the traditional setting where every node is a sink, and hence a location is covered if it simply lies within the range of some node. Then, drawing an analogy between the connected components of the network and the busy periods of an $M/D/\infty$ queue (and using renewal theoretic arguments) we derive a closed-form expression for the average vacancy (complement of coverage). We also compute an upper bound for vacancy by introducing the notion of *left-coverage* (i.e., coverage by a node on the left); a lower bound is derived by coupling our model with an *independent-disk model*, where the sinks' coverage regions are independent and identically distributed. Through an extensive theoretical and numerical study, we investigate the problem of minimizing network deployment cost subject to a constraint on the average vacancy. We also conduct simulations to understand the properties of a general notion of coverage, obtained by introducing hop-counts into the definition. Parameterized approximations for the hop-constrained cluster lengths (around a sink) are proposed, whose efficacy is evaluated numerically. In particular, there exists a range of parameter values where our cluster-length approximation is good. Finally, hop-constrained cost optimization is conducted to demonstrate the efficacy of the infrastructure-based design.**

***Index Terms*—Coverage of wireless networks, multihop wireless networks for IoT.**

I. Introduction

The Internet of Things (IoT) envisions embedded sensors (and even actuators) in all static and mobile objects and even humans and animals, for enabling applications such as condition monitoring, asset tracking, and resource monitoring, for the purposes of predictive maintenance, and performance management. The models we study in this paper, and the questions we ask with those models, are motivated by the future vision of installed wireless networks, within buildings or along streets, that will provide universal connectivity for quickly creating IoT applications. For example, in a hospital a well known problem is that of tracking the location of mobile diagnostic devices, and of monitoring patients who have diagnostic devices attached to their bodies [2], [3], while being allowed to move away from their beds. Factories and warehouses have similar problems of tracking small industrial vehicles, and mobile tools, and monitoring the location and well-being of the many employees who might work in dangerous situations. How do such organisations build out networks to provide universal coverage for IoT devices in their premises? The standardisation process of 5G cellular networks includes standards for connectivity of IoT devices; however, even the 5G technology vision envisions "capillary networks" that will feed into cellular IoT gateways [4]. Further, given the experience with two generations of cellular broadband services, cellular networks have not replaced local networks in home, offices, and factories. Thus, one expects that organisations will build their own wireless networks for supporting their IoT applications.

The cost of installation and the ease of retrofitting into existing large facilities are important considerations. The networks should be easy to install, and it should be easy and inexpensive to expand the networks as needs arise. Building out a complete infrastructure network, with wired access points providing full coverage might be difficult and very expensive; retrofitting and expanding such a network is difficult and costly. On the other hand, adding wireless relays to build out a network, or building a network comprising some wired access points and some wireless relays, with multihop wireless communications might be more cost effective and easily deployable. The models we study in this paper are motivated by this thinking.

Specifically, the setting we are interested in is the following. We consider a network comprising two types of static nodes – *sinks* and *relays*. The sink nodes are connected to an infrastructure backhaul, while the relay nodes are deployed so as to extend the network coverage by providing multi-hop connectivity to the sink nodes. Thus, a location is said to be *covered* if it lies within the communication range of some node that is *eventually connected (possibly via multiple hops) to a sink node*. A more general formulation is obtained by imposing *a constraint on the number of hops* within which a sink node can be reached; such a constraint would *model the delay requirements* of the applications that use the network [5]. The above characterization (of coverage and hop-constrained coverage) will be useful for network provisioning, where the objective is to minimize the average cost of the network subject to constraints on coverage and delay.

In this paper we develop the theory and analysis for one-dimensional networks (i.e., the sinks and the relays are deployed along a line, and the mobile sources of data are also on the line). Our model and the questions that we ask are

K. P. Naveen is with the Department of Electrical Engineering, Indian Institute of Technology Tirupati, Renigunta Road, Settipalli Post, Tirupati 517506, India (Email: naveenkp@iittp.ac.in); Anurag Kumar is with the Department of Electrical Communication Engineering, Indian Institute of Science, Bangalore 560012, India (Email: anurag@ece.iisc.ernet.in).

This work was supported by the Department of Science and Technology, Government of India, through an INSPIRE Faculty Award (K. P. Naveen) and a J. C. Bose National Fellowship (Anurag Kumar). The conference version of this work [1] has appeared in ACM MSWIM, held at Malta, Nov. 2016.

novel, and can provide direct insights for applications such as the following. (i) Patients recovering in hospitals may be allowed to walk freely in the hospital corridors, while carrying IoT-enabled monitoring devices such as blood oxymeters, and blood pressure monitors. Our one-dimensional network model can represent a long hospital corridor, the objective being that, as the patients walk along the corridor, they are "covered" by the network of sinks and relays. (ii) The one-dimensional model could also represent a straight road along the edge of which sinks and relays are deployed (on lamp-posts or other road-side infrastructure) so as to provide coverage for IoT-enabled sensors on the road surface (e.g., for human distress calls, or parking violations).

The outline of the paper is as follows. In Section II we survey related literature, following which we discuss our main technical contributions. In Section III we describe our infrastructure-based network model in detail. In Section IV we discuss the traditional case where every node is a sink. The general case, comprising both sink and relay nodes, is studied in Section V. In Section VI, we define a hop-count constrained notion of coverage. Numerical and simulation results are presented in Section VII. We finally summarize our work in Section VIII. Due to page-length restriction, derivation of some expressions and proofs of Theorem 2 and 3 are made available as *Supplementary Material*.

II. Related Work and Our Contribution

We will first discuss literature from coverage processes and its applications to wireless networks. Since coverage and connectivity are related, we will proceed to briefly introduce work from the latter topic. Next, we survey work related to one-dimensional networks, and then proceed to discuss literature on infrastructure-based networks. Finally, we place our work in context by highlighting our main technical contributions.

Traditional coverage processes have been extensively studied for the *Boolean model* which comprises nodes of only one type (or, in our terminology, comprises only sink nodes), with independent and identically distributed (i.i.d.) shapes (or coverage regions) placed around each node; the shapes are further independent of the node locations. A classical reference for this topic is the book by Hall [6]. In the context of wireless communication, the problem of coverage has been extended to the more general *SINR (Signal to Interference plus Noise Ratio) model* [7]–[9]. For instance, Andrews et al. in [7] consider the SINR model where the region covered by a node depends on its signal power as well as the interference power received from all other nodes. Formally, a location is covered by a node if the SINR received at the location is greater than a threshold value. The above setting is extended in [8] to a scenario where the nodes are heterogeneous in terms of their transmit power and their SINR threshold.

A quantity that is closely related to coverage is connectivity. A key result concerning connectivity in wireless networks is that by Gupta and Kumar [10]. Specifically, for a network deployed uniformly on an unit disk, to guarantee asymptotic connectivity they obtain the scale at which the (deterministic) transmission radius should reduce with the number of nodes. Connectivity results of similar asymptotic flavour are studied in [11], [12], while the problem of connectivity in the presence of channel randomness (so that the transmission radii are random) have been addressed in [13], [14]. The related problem of determining critical sensing radius in camera sensor networks has also been recently studied in the literature; see [15] and references therein.

All the above work, however, assumes that either all nodes are sinks so that coverage by any one node suffices, or seek multi-hop connectivity between every pair of nodes in the network. This is in contrast to our work where we introduce relay nodes, and define a point to be covered if and only if it has a multi-hop connectivity to at least one sink node; thus, relay nodes connected to different sinks may not have a multi-hop path between them. Although we assume a Boolean model like in [6], our work can be considered as an extension of the model in [6] to the infrastructure-based network setting, but restricted to the one-dimensional case.

There are already extensive work in the literature studying the problem of coverage and connectivity in one-dimensional networks. In the following we survey some of this work. For a network with a finite number of nodes deployed on a line of finite length, Desai and Manjunath in [16] obtain the exact formula for the probability that the entire network is connected. Miorandi and Altman in [17] adopt a queueing theoretic approach to compute the coverage probability for one-dimensional networks. For a general inter-node distance distribution (not limiting to exponential distribution), the authors in [17] show the equivalence between the coverage probability and the probability that an equivalent $GI/D/1$ queue is busy. We will establish a similar equivalence for the infrastructure-based network.

One early work considering an infrastructure-based architecture is that of Dousse et al. [18]. In [18], although the relay locations constitute the points of a Poisson process, the sink nodes are placed equi-distance from each other (which is in contrast to our work where the sink locations also constitute an independent Poisson process). A point located between two sink nodes is connected if it has a multi-hop path to at least one of them. Thus, the model essentially reduces to the one with two sink nodes placed at the end points of a finite-length line segment. The authors in [18] obtain a lower bound on the probability that a location within the line segment is connected. For a similar model, motivated by vehicular networks, Suo in [19] obtains the probability that all vehicles (equivalently, relay nodes) within a road segment of finite length are connected to both *road side units* (equivalently, sink nodes) located at either ends of the road segment.

Recently, Ng et al. in [20] consider a model where more than two sink nodes are deployed at arbitrary locations within a segment of finite length; the relay nodes are Poisson distributed as in the earlier models. The probability that the entire network is connected is obtained. Further, the authors show that uniform sink placement maximizes the connectivity probability. Assuming different ranges for sink and relay nodes, Zhang et al., in [21], obtain the uplink (relay to sink) and downlink (sink to relay) connection probabilities. However, the setting is again restricted to the scenario where two sink nodes are place at the either ends of a finite length line segment.

In contrast to all the above work, we consider a model where the locations of both sink and relay nodes constitute the points of two independent Poisson processes. We are interested in obtaining explicit expression for the fraction of region that is covered (i.e., coverage probability) as a function of sink and relay node densities. To the best of our knowledge, the particular model we consider and the coverage characterization we obtain are not available in the literature. Our main technical contributions are as follows:

1) **Expression for Average Vacancy[1]:** Using renewal theoretic arguments we derive an explicit closed-form expression for the average vacancy created in an infrastructure-based network (Theorem 1). The above result can be considered as a generalization of the classical expression for average vacancy known in the literature of coverage processes.
2) **Bounds on Average Vacancy:** Defining *left-coverage*[2] we obtain an upper bound for the average vacancy. More interesting, we show that the average vacancy created in an alternate Boolean model (where the coverage regions of successive sink nodes are independent and identically distributed), serves as a lower bound for the average vacancy in the original model (Theorem 2).
3) **Network-cost Optimization:** We formulate the problem of minimizing the network deployment cost (average unit-length cost of the network) subject to a constraint on the average vacancy. We conduct a theoretical analysis to investigate convexity properties of the above formulation (Lemma 3). Further properties of network optimization is derived through an extensive numerical study.
4) **Hop-constrained Coverage:** We conduct simulation experiments to study the average vacancy created in a hop-count constrained model. We also propose approximations for the length of the cluster around a sink node (Theorem 3). The performance of the proposed approximations are numerically validated.

III. System Model

We consider a scenario where the sink and the relay nodes are located along a line. The point process of these locations is modeled as a Poisson process of rate λ. It is assumed that any point of this Poisson process is independently a sink with probability $\beta \in (0, 1]$. Thus, the point processes of sink locations and relay locations are independent Poisson processes of rates $\beta\lambda$ and $(1-\beta)\lambda$, respectively. The wireless *range* of each node is $r > 0$. Thus, we assume that the ranges of both sink and relay nodes are identical. This assumption can be justified by considering scenarios where both sink and relay nodes are equipped with identical digital radios, while the sink nodes have additional (high speed) backhaul connectivity (e.g., ethernet or satellite radios).

Remark: The *one-dimensional setting* could model a long corridor in a large building, a long underground tunnel under a dam or in a mine, or a long straight stretch of road. Regarding *random (Poisson) deployment* assumption, we note that it is commonly employed in literature [7]–[14], [16]–[18], particularly when the network under consideration is deployed in an ad hoc fashion. Even in scenarios where the deployment is planned, nodes are generally not deployed at regular intervals, due to the physical constraints on where the wireless nodes can be placed. For example, along the ceiling of a building corridor, other infrastructure, such as vents, lights, and pillars, would govern the availability of spaces for mounting wireless network nodes. Thus, assuming a one-dimensional deployment, the locations of the sinks and the relays can be viewed as a realisation of a point-process along a line. For mathematical tractability, we have used a homogeneous Poisson point process model. A comparison of point process models for cellular base-station placements has been performed by Andrews et al. [22], where they have compared cellular coverage obtained from a Poisson model and a grid model, with coverage obtained from an actual deployment. They conclude that the Poisson model yields conservative results, while providing closed form solutions and, therefore, more insight. For instance, in our context the Poisson assumption enables us to derive a closed form expression for vacancy (see (19)), using which we will be able to gain valuable insights about the coverage properties of infrastructure-based networks (via our numerical work in Section VII). We would like to however emphasize that more involved deployment models (other than Poisson) such as the *Cluster (Cox) process* (which is useful for modeling situations where base-stations are likely to be close to one another, e.g., due to terrain) are available in the literature [23].

A. Connectivity

Given two nodes whose locations are x and y ($x \neq y$), we say that the *nodes are connected* if, for some $h \geq 1$, there are nodes at locations $x_0 = x, x_1, \cdots, x_h = y$, such that $|x_{i-1} - x_i| \leq r$ for $i = 1, \cdots, h$; otherwise the nodes are said to be *disconnected*.

We define a *connected component*, $\mathcal{C}$, to be the maximal set of nodes such that any pair of nodes in the set are connected. Formally, $\mathcal{C}$ is a connected component if (i) u and v are connected for all $u, v \in \mathcal{C}$, and (ii) u and w are disconnected for all $u \in \mathcal{C}$ and $w \notin \mathcal{C}$.

Since we are working with an infrastructure-based network, a node is operationally useful only if it is eventually connected to a sink node. Thus, we introduce the following definition: A node is said to be *sink-connected* if it is connected to at least one sink node; otherwise we say that the node is *sink-disconnected*. Formally, a node u is sink-connected if and only if there exists a sink node s and a connected component $\mathcal{C}$ such that $u \in \mathcal{C}$ and $s \in \mathcal{C}$. For instance, node u in Fig. 1 is sink-connected, while node v is sink-disconnected. Note that, by definition a sink node is always sink-connected.

B. Coverage and Vacancy

We finally introduce the definition of coverage for an infrastructure-based wireless network.

Definition 1: A location $\ell \in \Re_+$ is said to be **covered** if it is within the range of a sink-connected node; otherwise ℓ is said to be **vacant**.

[1] Vacancy is the complement of coverage; A location is said to be covered if it lies within the range of some node that is eventually connected (via. multi hopping) to a sink node.

[2] A location is said to be left-covered if it is covered by a sink-connected node (i.e., a node connected to the sink) to its left.

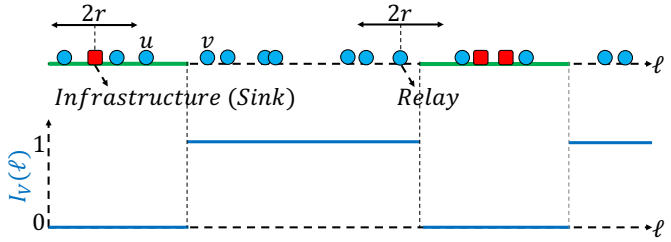

Fig. 1. An illustration of the covered and vacant regions.

Let $\mathcal{I}_V : \Re_+ \to \{0,1\}$ denote the indicator function that represents whether a location $\ell \in \Re_+$ is vacant or not. Formally, $\mathcal{I}_V(\ell) = 1$ if ℓ is vacant; $\mathcal{I}_V(\ell) = 0$ otherwise (i.e., if ℓ is covered); see Fig. 1 for an illustration. Then, the *average vacancy* (i.e., fraction of vacant region) created in the infrastructure-based wireless network (of node intensity λ and sink probability β) is given by,

$$v_{\lambda,\beta} = \lim_{L\to\infty} \frac{1}{L} \int_0^L \mathcal{I}_V(\ell) \mathrm{d}\ell. \tag{1}$$

By identifying renewal points in the network, it is possible to establish that the above limit exists a.s. (almost surely). For instance, locations of the sink nodes constitute one set of renewal points. Formally, if $\{Y_k : k \geq 1\}$ are the locations of the successive sink nodes (define $Y_0 = 0$) then the inter-sink distances, $\{X_k = Y_k - Y_{k-1} : k \geq 1\}$, is a *renewal sequence*. Define the *reward* in the k-th renewal cycle ($k \geq 1$) as,

$$R_k = \int_{Y_{k-1}}^{Y_k} \mathcal{I}_V(\ell) \mathrm{d}\ell. \tag{2}$$

Note that, $\{R_k : k \geq 1\}$ is an i.i.d. sequence since R_k is a function solely of the Poisson points located within the k-th renewal cycle. Thus, using renewal reward theory (RRT) [24], [25] we have,

$$v_{\lambda,\beta} = \frac{\mathbb{E}[R_k]}{\mathbb{E}[X_k]} \text{ a.s.} \tag{3}$$

Although the above procedure provides an expression for $v_{\lambda,\beta}$, it is not a workable definition as it is not easy to obtain an explicit formula for $\mathbb{E}[R_k]$ when $\beta \in (0,1)$ ($\beta = 1$ case can be easily solved; see Section IV). Thus, our objective is to identify alternative renewal points that can enable us to characterize $v_{\lambda,\beta}$ as an explicit function of (λ, β); see Section V.

C. Network Optimization

Finally, we are interested in deploying a cost efficient network. Suppose c_S and c_R denote the costs of a sink and a relay node, respectively. Then, the average (per unit-length) cost of the network is, $c_{\lambda,\beta} := \lambda\beta c_S + \lambda(1-\beta)c_R$. The objective is to minimize the average network cost subject to an average vacancy constraint:

$$\begin{array}{ll} \text{Minimize}_{(\lambda,\beta)} & c_{\lambda,\beta} \\ \text{Subject to} & v_{\lambda,\beta} \leq \overline{v}. \end{array} \tag{4}$$

The optimal network cost is denoted as c_{λ^*,β^*} where (λ^*, β^*) represents an optimal point. Convexity properties of the above problem, and an equivalent unconstrained formulation, will be discussed in Section V-C.

IV. Average Vacancy: $\beta = 1$ Case

This section is essentially a review of some existing results. Although the expression for average vacancy (when $\beta = 1$) is well known from the literature on coverage processes, the queueing theoretic approach for deriving the same is however more recent. Since we will be adopting the latter approach to tackle the general case where $\beta < 1$ (in Section V), this review will enable us to setup the basic framework that will be extended in the subsequent section.

The case $\beta = 1$ corresponds to a situation where every node is a sink. Thus, a location $\ell \in \Re_+$ is covered if it is simply within the range, r, of some node. Standard results from coverage processes [6] can now be evoked to obtain the average vacancy as $v_{\lambda,1} = e^{-\lambda 2r}$, where $2r$ is the length of the disk around each node (because the range on either side of a node is r; see Fig. 1).

The above result can also be obtained using (3) as follows. First, note that a location ℓ in the k-th renewal cycle is vacant only if it is not within the range r of both sinks at either ends of this cycle (i.e., nodes at Y_{k-1} and Y_k). Hence, the reward expression in (2) can be expressed as $R_k = (X_k - 2r)^+$, where $(x)^+ = \max\{0, x\}$. Next, since $\{X_k\}$ are exponential random variables of rate λ, the average reward and average renewal cycle length are given by,

$$\mathbb{E}[R_k] = \frac{e^{-\lambda 2r}}{\lambda} \text{ and } \mathbb{E}[X_k] = \frac{1}{\lambda}.$$

Thus, from (3) we have $v_{\lambda,1} = e^{-\lambda 2r}$.

As mentioned earlier, the above technique is not useful when $\beta < 1$ since it is then not easy to obtain an explicit expression for $\mathbb{E}[R_k]$. This motivates us to look for alternate renewal sequences. One idea is to view the successive covered and vacant regions in the network as being analogous to the successive busy and idle periods in an $M/D/\infty$ queuing system [24]. Then, recognizing that the start-instants of the busy periods constitute renewal points, the average vacancy expression can be alternatively obtained using results from $M/D/\infty$ queues [17]. Details are discussed below.

Borrowing terminology from queuing theory, we identify the *busy* and *idle* periods of an infrastructure-based network as follows. Let $\mathcal{C}_k$ be the k-th connected component with the positions of the leftmost and the rightmost nodes in $\mathcal{C}_k$ being denoted as x_k and y_k, respectively (see Fig. 2 for an illustration). Note that, if the node locations are thought as the times at which customers arrive into an $M/D/\infty$, then x_k represents the instance at which the k-th busy period starts while $y_k + r$ is the time at which the respective busy period ends. Formally, we define the *busy period* corresponding to $\mathcal{C}_k$ as the region $[x_k, y_k + r]$, while the *idle period* of $\mathcal{C}_k$ is the region $(y_k + r, x_{k+1})$, where x_{k+1} is the location of the leftmost node in the next connected component $\mathcal{C}_{k+1}$. Note that, unlike in queues where the idle periods are truly idle,

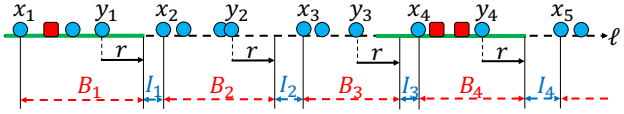

Fig. 2. Busy-idle periods in an infrastructure-based wireless network.

here it is possible that some locations within the idle period are covered by the first node in the next busy period, provided that the next busy period contains a sink node. Finally, Let B_k and I_k, $k \geq 1$, denote the lengths of the busy and idle periods corresponding to the k-th connected component, respectively.

We refer to the k-th busy-idle period as the k-th renewal cycle. Thus, $B_k + I_k$ is the length of the k-th renewal cycle. The reward in the k-th renewal cycle, denoted R'_k, is the fraction of region vacant in the k-th cycle. R'_k can be evaluated as follows. First, note that when $\beta = 1$ the busy periods are always completely covered since every node is a sink. Next, when the length of an idle period is less than r then the idle period is completely covered by the first node in the next busy period. Thus R'_k is simply the portion of the idle period that is not covered, which is given by $R'_k = (I_k - r)^+$.

The renewal cycle lengths, $\{B_k + I_k : k \geq 1\}$, is an i.i.d. sequence. The reward sequence, $\{R'_k : k \geq 1\}$, is also i.i.d. Hence, RRT can be applied to obtain

$$v_{\lambda,1} \quad = \quad \frac{\mathbb{E}[(I_k - r)^+]}{\mathbb{E}[B_k] + \mathbb{E}[I_k]} \text{ a.s.} \tag{5}$$

Since I_k is an exponentially distributed random variable of rate λ, we have $\mathbb{E}[I_k] = \frac{1}{\lambda}$ and $\mathbb{E}[(I_k - r)^+] = \frac{e^{-\lambda r}}{\lambda}$. $\mathbb{E}[B_k]$ is the average busy period of an $M/D/\infty$ queuing system with constant service times r, which is given by [17]

$$\mathbb{E}[B_k] = r + \frac{\int_0^r t f_X(t) dt}{1 - F_X(r)}$$

where f_X and F_X are the p.d.f. and c.d.f., respectively, of the inter-arrival times. The inter-arrival times in our case are the inter-node distances, which are exponentially distributed random variables of rate λ, i.e., $f_X(t) = \lambda e^{-\lambda t}$ and $F_X(r) = (1 - e^{-\lambda r})$. Hence, we have

$$\mathbb{E}[B_k] = \frac{(1 - e^{-\lambda r})}{\lambda e^{-\lambda r}}. \tag{6}$$

Using the above quantities in (5), we obtain $v_{\lambda,1} = e^{-\lambda 2r}$.

V. Average Vacancy: $\beta < 1$ Case

The case $\beta < 1$ yields an infrastructure-based network, comprising both sink and relay nodes. Here, a location within the range of a relay node is covered if and only if the relay is connected to a sink node. We will first argue that the earlier approach (employed for the $\beta = 1$ case) of regarding the successive busy-idle periods as renewal cycles is not applicable when $\beta < 1$; however, a simple upper bound can be derive using this approach. We hence proceed to seek alternate renewal epochs that will enable us to derive the average vacancy for this case. The details are presented in the following.

Continuing the discussion from the previous section, when $\beta < 1$, it is possible for a connected component to not contain a sink node (for instance, $\mathcal{C}_2$ and $\mathcal{C}_3$ in Fig. 2 does not contain sink nodes). Hence, the corresponding busy period must be treated as being vacant.Let $\mathcal{S}_k$ denote the event that there exists a sink in the k-th connected component. Let $\mathcal{S}_k^c$ be the complement of $\mathcal{S}_k$. Note that the events $\mathcal{S}_k, k \geq 1$, are independent and have the same probability.

Unlike in the $\beta = 1$ case, here it is not useful to regard the successive busy-idle periods as renewal cycles. This is because the reward R'_k, which is the fraction of region uncovered within the k-th busy-idle period, is given by ($\mathbb{I}_A$ denotes the indicator function of event A)

$$R'_k \quad = \quad \begin{cases} B_k + I_k & \text{if} \quad \mathbb{I}_{\mathcal{S}_k^c \cap \mathcal{S}_{k+1}^c} = 1 \\ B_k + I_k - r & \text{if} \quad \mathbb{I}_{\mathcal{S}_k^c \cap \mathcal{S}_{k+1}} = 1 \\ I_k & \text{if} \quad \mathbb{I}_{\mathcal{S}_k \cap \mathcal{S}_{k+1}^c} = 1 \\ (I_k - r)^+ & \text{if} \quad \mathbb{I}_{\mathcal{S}_k \cap \mathcal{S}_{k+1}} = 1. \end{cases} \tag{7}$$

We see that the reward in the k-th busy-idle period depends on whether or not the $(k+1)$-th busy-idle period contains a sink node. Thus, unlike the $\beta = 1$ case, the reward sequence $\{R'_k : k \geq 1\}$ is not i.i.d. As a consequence, RRT cannot be applied to write $v_{\lambda,\beta} = \mathbb{E}[R'_k]/(\mathbb{E}[B_k] + \mathbb{E}[I_k])$ (as in (5)), although it is possible to compute $\mathbb{E}[R'_k]$ using $\mathbb{P}(\mathcal{S}_k)$[3]

A simple upper bound for vacancy can however be obtained by neglecting the region covered by the $(k+1)$-th busy period in the reward expression for R'_k (in case a sink is present in the corresponding connected component). We derive this upper bound first (in Section V-A) before proceeding to obtain the exact expression for vacancy (in Section V-B). In Section V-D we prove a lower bound for vacancy by coupling our model with a traditional Boolean model where i.i.d. coverage disks are placed around the sink nodes.

A. An Upper Bound for Vacancy

We begin with the following definition.

Definition 2: A location $\ell \in \Re_+$ is said to be covered from the left or **left-covered** if ℓ is within the range of a sink-connected node towards the left of ℓ, i.e., ℓ is left-covered if there is a sink-connected node at some location x such that $x \leq \ell$ and $|x - \ell| \leq r$. If there is no such sink-connected node we say that ℓ is vacant from the left or **left-vacant**.

Let $\mathcal{I}_U : \Re_+ \to \{0, 1\}$ denote the function indicating whether a location $\ell \in \Re_+$ is left-vacant or not. Then, the fraction of region that is left-vacant is given by,

$$u_{\lambda,\beta} = \lim_{L \to \infty} \frac{1}{L} \int_0^L \mathcal{I}_U(\ell) \mathrm{d}\ell. \tag{8}$$

We immediately obtain the following result.

Lemma 1: The fraction of left-vacant region is an upper bound for the fraction of vacant region, i.e., $v_{\lambda,\beta} \leq u_{\lambda,\beta}$ for all (λ, β).

Proof: Note that, for any $\ell \in \Re_+$ we have

$$\mathcal{I}_V(\ell) \leq \mathcal{I}_U(\ell).$$

The above relation can be easily deduced by noting that ℓ being vacant ($\mathcal{I}_V(\ell) = 1$) always implies that ℓ is left-vacant ($\mathcal{I}_U(\ell) = 1$). However, it is possible that ℓ is covered by a node towards its right ($\mathcal{I}_V(\ell) = 0$), but is not left-covered ($\mathcal{I}_U(\ell) = 1$). Thus, $v_{\lambda,\beta}$ is upper bounded by $u_{\lambda,\beta}$. ■

We now proceed to obtain an explicit expression for $u_{\lambda,\beta}$.

[3]Note that, since $\mathcal{S}_k$ and $\mathcal{S}_{k+1}$ are i.i.d. events, we have $\mathbb{P}(\mathcal{S}_k \cap \mathcal{S}_{k+1}) = \mathbb{P}(\mathcal{S}_k)\mathbb{P}(\mathcal{S}_{k+1}) = \mathbb{P}(\mathcal{S}_k)^2$. The probability of other events can be computed similarly; for instance, $\mathbb{P}(\mathcal{S}_k^c \cap \mathcal{S}_{k+1}) = (1 - \mathbb{P}(\mathcal{S}_k))\mathbb{P}(\mathcal{S}_k)$. Thus, the expectation of the reward R'_k in (7) can be computed using $\mathbb{P}(\mathcal{S}_k)$.

Lemma 2: For any given (λ, β), the fraction of left-vacant region is given by

$$u_{\lambda,\beta} = \frac{1 + \lambda\beta r + \beta^2\left(e^{\lambda r} - \lambda r - 1\right)}{\left(1 - \beta + \beta e^{\lambda r}\right)^2}. \tag{9}$$

Proof: We begin by regarding the busy-idle periods corresponding to the k-th connected component as the k-th renewal cycle. Let the reward in the k-th renewal cycle, denoted R''_k, be the length of the region that is left-vacant. Then,

$$R''_k = B_k \mathbb{I}_{\mathcal{S}_k^c} + I_k. \tag{10}$$

The sequence $\{R''_k : k \geq 1\}$ is i.i.d. unlike the $\{R'_k : k \geq 1\}$ sequence in (7). Hence, we can now apply RRT to obtain

$$u_{\lambda,\beta} = \frac{\mathbb{E}[B_k \mathbb{I}_{\mathcal{S}_k^c}] + \mathbb{E}[I_k]}{\mathbb{E}[B_k] + \mathbb{E}[I_k]}. \tag{11}$$

For notational simplicity, define $p := \mathbb{P}(\mathcal{S}_k^c)$ and $Q := \mathbb{E}[B_k|\mathcal{S}_k^c]$. Thus, p is the probability that a connected component does not contain a sink, and Q is the average busy period length conditioned on the event that it does not contain a sink. Hence, we have

$$\mathbb{E}[B_k \mathbb{I}_{\mathcal{S}_k^c}] = \mathbb{P}(\mathcal{S}_k^c)\mathbb{E}[B_k \mathbb{I}_{\mathcal{S}_k^c}|\mathcal{S}_k^c] = pQ$$

Substituting the above expression in (11) along with the identities $\mathbb{E}[I_k] = \frac{1}{\lambda}$ and $\mathbb{E}[B_k] = \frac{1-e^{-\lambda r}}{\lambda e^{-\lambda r}}$, we obtain

$$u_{\lambda,\beta} = \left(\lambda p Q + 1\right) e^{-\lambda r}. \tag{12}$$

Explicit formulas for p and Q along with $\overline{Q} = \mathbb{E}[B_k|\mathcal{S}_k]$ (which will be required in our subsequent development) are derived in Supplementary Material; we recall the expressions for these here for convenience (as well as for completeness):

$$p = 1 - q = \frac{(1-\beta)e^{-\lambda r}}{\beta + e^{-\lambda r} - \beta e^{-\lambda r}} \tag{13}$$

$$Q = p\mathbb{E}[B_k] + (1-p)r \tag{14}$$

$$\overline{Q} = \frac{\mathbb{E}[B_k] - pQ}{(1-p)}. \tag{15}$$

Substituting for p and Q from the above expressions in (12), and simplifying[4] yields the result in (9). ∎

B. Exact Vacancy Analysis

To obtain $v_{\lambda,\beta}$ exactly we identify alternate renewal instances. Specifically, as illustrated in Fig. 3, we regard the end points of the sink-containing busy periods as renewal instances. Thus, a renewal cycle starts with an idle period while comprising a random number of successive non-sink-containing busy-idle periods, and finally ends with a sink-containing busy period.

Let M_n denote the number of busy periods (both non-sink and sink containing) within the n-th renewal cycle. Thus,

[4]Since manual simplification is cumbersome, we have used *Mathematica* to simplify the expression in (12)

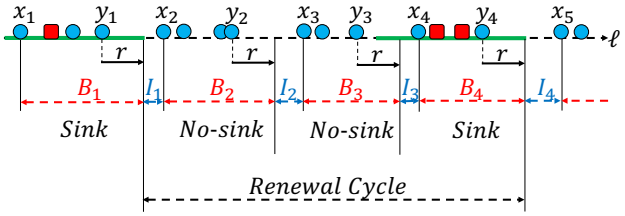

Fig. 3. Illustration of a renewal cycle when $\beta < 1$.

$M_n = m$ $(m \geq 1)$ implies that the first idle period is followed exactly by $(m-1)$ successive non-sink-containing busy-idle periods, while the renewal cycle ends with the m-th busy period which invariably contains a sink; thus, counting the first idle period and the last busy period, the corresponding renewal cycle contains M_n busy-idle periods in total. Note that, M_n is a geometric random variable with success probability $q := \mathbb{P}(\mathcal{S}_k) = 1 - p$. Thus, we have

$$\mathbb{P}(M_n = m) = (1-q)^{m-1}q, \quad \text{for } m \geq 1. \tag{16}$$

Let $I_i^{(n)}$ and $B_i^{(n)}$ $(1 \leq i \leq M_n)$ denote the lengths of the i-th idle and busy periods within the n-th renewal cycle. Then, the length of the n-th renewal cycle is given by,

$$\hat{X}_n = \sum_{i=1}^{M_n} \left(I_i^{(n)} + B_i^{(n)}\right). \tag{17}$$

The reward $\hat{R}_n$ is simply the length of the vacant region within the n-th renewal cycle, which can be expressed as

$$\hat{R}_n = \begin{cases} \left(I_1^{(n)} - r\right)^+ & \text{if } M_n = 1 \\ \sum_{i=1}^{M_n - 1}\left(I_i^{(n)} + B_i^{(n)}\right) + I_{M_n}^{(n)} - r & \text{if } M_n > 1. \end{cases} \tag{18}$$

We are ready to state and prove the following key theorem:

Theorem 1: For any given (λ, β), the fraction of vacant region is given by

$$v_{\lambda,\beta} = \frac{1}{\left(1 - \beta + \beta e^{\lambda r}\right)^2} \tag{19}$$

Proof: We now proceed to compute the expectation of the above quantities. For simplicity, define $\overline{Q} := \mathbb{E}[B_k|\mathcal{S}_k]$, which is the average length of the busy period, conditioned on the event that it contains a sink node. The expectation of $\hat{X}_n$ can be simplified as follows:

$$\begin{aligned}
\mathbb{E}[\hat{X}_n] &= \mathbb{E}\left[\sum_{i=1}^{M_n}\left(I_i^{(n)} + B_i^{(n)}\right)\right] \\
&= \sum_{m=1}^{\infty} \mathbb{P}(M_n = m)\ \mathbb{E}\left[\sum_{i=1}^{M_n}\left(I_i^{(n)} + B_i^{(n)}\right)\middle| M_n = m\right] \\
&\overset{(a)}{=} \sum_{m=1}^{\infty} \mathbb{P}(M_n = m)\left(\frac{m}{\lambda} + (m-1)Q + \overline{Q}\right) \\
&= \sum_{m=1}^{\infty} (1-q)^{m-1} q \left(\frac{m}{\lambda} + (m-1)Q + \overline{Q}\right) \\
&\overset{(b)}{=} \frac{1}{\lambda q} + \left(\frac{1-q}{q}\right) Q + \overline{Q}
\end{aligned}$$

$$\stackrel{(c)}{=} \frac{\left(1-\beta+\beta e^{\lambda r}\right)}{\lambda\beta}. \tag{20}$$

To obtain (a) note that, conditioned on $(M_n = m)$, the mean length of each of the m idle periods is $\frac{1}{\lambda}$; the first $(m-1)$ busy periods do not contain a sink (the average length of each is Q) while the last busy period contains a sink (whose average length is $\overline{Q}$). Equality (b) is obtained using the following identities (corresponding to the geometric distribution):

$$\sum_{m=1}^{\infty}(1-q)^{m-1}q = 1, \quad \sum_{m=1}^{\infty} m(1-q)^{m-1}q = \frac{1}{q}.$$

Substituting for p, Q and $\overline{Q}$ (from (13), (14) and (15)) and simplifying (using *Mathematica*) yields the final equality (c).

Similarly, conditioning on $(M_n = m)$ and simplifying, we obtain the following expression for $\mathbb{E}[\hat{R}_n]$:

$$\mathbb{E}[\hat{R}_n] = \mathbb{P}(M_n = 1)\frac{e^{-\lambda r}}{\lambda} + \sum_{m=2}^{\infty}\mathbb{P}(M_n = m)\times \left(\frac{m}{\lambda} + (m-1)Q - r\right)$$

$$= \frac{q^2 e^{-\lambda r} + \lambda p Q - pq\lambda r + p(1+q)}{\lambda q}.$$

$$= \frac{1}{\lambda\beta\left(1-\beta+\beta e^{\lambda r}\right)}. \tag{21}$$

RRT can now be evoked to express the average vacancy as $v_{\lambda,\beta} = \frac{\mathbb{E}[\hat{R}_n]}{\mathbb{E}[\hat{X}_n]}$, which, using (20) and (21), can be simplified to yield the expression in (19). ∎

Discussion: Note that the expression for $v_{\lambda,\beta}$ in (19) encompasses the $\beta = 1$ case. This is easy to verify, as substituting $\beta = 1$ in (19) yields $v_{\lambda,1} = e^{-\lambda 2r}$. On the other hand, as $\beta \to 0$ we see that $v_{\lambda,\beta} \to 1$; this result should not be surprising as well because, as the density of sink nodes reduces to 0, the network is expected to be rendered completely vacant. In general, for any $\beta \in (0,1]$, the average vacancy $v_{\lambda,\beta}$ can be easily computed using the expression in (19). Our study thus generalizes the traditional coverage processes model (comprising only sink nodes) to the infrastructure-based setting (where both sink and relay nodes are present).

We next proceed to investigate the convexity properties of the average vacancy expression in (19). The results are reported in the following lemma.

Lemma 3: (a) For a given β, $v_{\lambda,\beta}$ is a decreasing function of λ. Similarly, for a given λ, $v_{\lambda,\beta}$ is decreasing in β.
(b) $v_{\lambda,\beta}$ is neither convex nor concave.
(c) $v_{\lambda,\beta}$ is quasi-convex but not quasi-concave.

Proof: Available in the Supplementary Material. ∎

C. Simplification of the Network Optimization Problem

Using the results in Lemma 3, we can infer the following about the network optimization problem in (4). The problem in (4) is non-convex since $v_{\lambda,\beta}$ is non-convex (Lemma 3 (b)). Although $v_{\lambda,\beta}$ is quasi-convex (Lemma 3 (c)), the cost function $c_{\lambda,\beta}$ is however quasi-concave (proof of this result is available in the Supplementary Material). As a result the problem in (4) cannot be posed as a quasi-convex problem as well. However, using the monotonicity results in Lemma 3 (a) it is possible to simplify the problem in (4) into an equivalent unconstrained problem. For this, we first require the following result that shows that the inequality constraint in (4) is tight at optimal points.

Lemma 4: If (λ^*, β^*) is an optimal point for the problem in (4), then $v_{\lambda^*,\beta^*} = \overline{v}$.

Proof: Suppose $v_{\lambda^*,\beta^*} < \overline{v}$, then Lemma 3 (a) suggests that the vacancy constraint can be met by either decreasing λ^*, or β^* (or a combination of both). This would however reduce the optimal cost c_{λ^*,β^*}, thus contradicting the hypothesis that (λ^*, β^*) is an optimal point. Hence, we have $v_{\lambda^*,\beta^*} = \overline{v}$. ∎

An important consequence of the above result is that the inequality constraint in (4) can be replaced by the equality constraint $v_{\lambda,\beta} = \overline{v}$. Now, for a given β, the value of λ (denoted $\lambda(\beta)$) required to achieve a target vacancy of $\overline{v}$ is obtained by solving $v_{\lambda(\beta),\beta} = \overline{v}$. The solution is given by

$$\lambda(\beta) = \frac{1}{r}\ln\left(1+\frac{\tilde{v}}{\beta}\right) \tag{22}$$

where $\tilde{v} = \frac{1-\sqrt{\overline{v}}}{\sqrt{\overline{v}}}$. Thus, using $\lambda(\beta)$ in the expression of the cost function, the *original problem* in (4) can be reduced to the following equivalent *unconstrained problem*:

$$\underset{\beta(0,1]}{\text{Minimize:}} \quad c(\beta) \tag{23}$$

where

$$c(\beta) := c_{\lambda(\beta),\beta} = \frac{1}{r}\ln\left(1+\frac{\tilde{v}}{\beta}\right)\Big(\beta c_S + (1-\beta)c_R\Big). \tag{24}$$

We use β^* to denote an optimal point. Thus, the optimal cost is given by $c_{\lambda^*,\beta^*} = c(\beta^*)$ where $\lambda^* = \lambda(\beta^*)$.

Finally, we study the convexity properties of the function $c(\beta)$ in (24). In Fig. 4 we plot $c(\beta)$ vs. β for different values of c_S and $\overline{v}$. We immediately observe the $c(\beta)$ is non-convex for some values of c_S and $\overline{v}$; for instance, see the plot corresponding to $c_S = 10c_R$ in Fig. 4(a). Hence, in general, the unconstrained problem in (23) is non-convex. However, from Fig. 4 we notice that $c(\beta)$ is either strictly decreasing or strictly unimodal, thus suggesting that $c(\beta)$ is strictly quasi-convex [26]. Although we have not been able to prove (or disprove) this result, the compelling evidence from our numerical work motivates us to conjecture this observation.

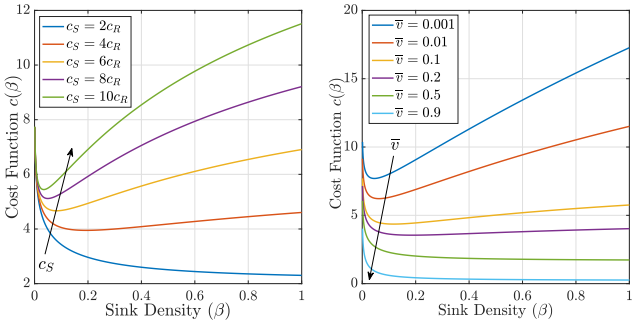

(a) (b)

Fig. 4. $c(\beta)$ vs. β curves for (a) different values of c_S with $\overline{v} = 0.1$ (b) for different values of $\overline{v}$ with $c_S = 5c_R$. In both cases, we have fixed $c_R = 1$.

Conjecture 1: $c(\beta)$ in (24) is strictly quasi-convex.

The validity of the above conjecture is also verified while conducting a detailed numerical study in Section VII-B.

A consequence of the above conjecture is that the unconstrained problem in (23) is strictly quasi-convex. Thus, there exists a unique solution β^* to the unconstrained problem [26]. Since the unconstrained and the original problems are equivalent, we can claim that there is a unique solution (λ^*, β^*) (where $\lambda^* = \lambda(\beta^*)$) to the latter problem as well. In Section VII-B we will conduct a detailed numerical study to understand the properties of the optimal solution.

D. A Lower Bound for Vacancy

In this section we will show that the average vacancy in an *independent-disk model*, which is obtained by placing i.i.d. coverage regions (or disks) around the sink nodes, will serves as a lower bound for the average vacancy in the original model (henceforth referred to as the *dependent-disk model*) where the coverage disks are not independent. We begin by introducing some notation.

Let $Y_k \in \Re_+$ ($k \geq 1$) denote the location of the k-th sink node. For simplicity, with a slight abuse of notation we will use Y_k to also refer to the k-th sink node. Defining $X_k = Y_k - Y_{k-1}$ (with $Y_0 = 0$), note that $\{X_k : k \geq 1\}$ constitutes a Poisson (renewal) process of rate $\beta\lambda$. The location of the relay nodes are instead represented using Λ, where Λ is a Poisson (counting) process of rate $(1-\beta)\lambda$ (i.e., for any interval I, $\Lambda(I)$ denotes the number of points within I). To avoid boundary effects occurring at the origin, let us assume that the relays are distributed along the entire real line. Thus, Λ is a Poisson process on $\Re$.

Definition 3: Retaining Y_k and the relay nodes, remove all other sink nodes from the network. Then, the ***relay-extended coverage disk*** (or simply the *coverage disk*) of Y_k is defined as the set of all locations that are either

- directly within the range of Y_k, or
- within the range of some relay that is connected to Y_k.

Let U_k (respectively, V_k) denote the length of the coverage disk towards the right (respectively, left) of Y_k. Thus, the coverage disk of Y_k is the region $\mathcal{W}_k := [Y_k - V_k, Y_k + U_k]$.

Given that the relay nodes are distributed according to Λ, U_k is simply the length of the busy period duration of an $M/D/\infty$ queue with arrival rate $(1-\beta)\lambda$ and constant service times r. Recalling (6), the average length of U_k can be written as

$$\overline{C} := \mathbb{E}[U_k] = \frac{(1 - e^{-(1-\beta)\lambda r})}{(1-\beta)\lambda e^{-(1-\beta)\lambda r}}. \tag{25}$$

Since the process Λ is i.i.d. on either side of Y_k, it follows that V_k is independent and identically distributed as U_k. Thus, the average length of the coverage disk around Y_k is $2\overline{C}$. However, as mentioned earlier, the coverage disks around Y_k and Y_{k+1}, although identically distributed, are not independent. This is because these disks are constructed using the same Poisson process, Λ, of relay nodes. Hence, we refer to our original model as the *dependent-disk model*.

Now, suppose we consider an alternate *independent-disk model* where, in fact, i.i.d. coverage disks of mean length $2\overline{C}$ are placed around the sink nodes. Then, we are in the regime of the traditional coverage processes with grain density $\beta\lambda$ and disk length $2\overline{C}$. Let $w_{\lambda,\beta}$ denote the fraction of vacancy created in this coverage process. Then, from [6] we have

$$w_{\lambda,\beta} = e^{-\beta\lambda 2\overline{C}}. \tag{26}$$

We show that $w_{\lambda,\beta}$ is a lower bound for $v_{\lambda,\beta}$.

Theorem 2: Fraction of vacancy created in the independent-disk model is a lower bound for that created in the dependent-disk model, i.e., $w_{\lambda,\beta} \leq v_{\lambda,\beta}$ for all (λ, β).

Proof Outline: The proof is based on a coupling argument. Given the dependent-disk model, we will iteratively construct an independent-disk model such that the region covered by the latter is larger. In fact, we will show that a larger coverage is obtained by placing i.i.d. coverage disks around a carefully chosen subset, $\{Y_{k_n} : n \geq 1\}$, of sink nodes. The details are available in Supplementary Material. ■

Remark: The coupling argument used to derive the lower bound result in Theorem 2 may be extended to higher dimensions. Thus, the result derived in this section can serve as a useful lower bound for vacancy in infrastructure-based networks in two-dimensional networks where it may not be possible to obtain an explicit expression for exact vacancy.

VI. Hop-Constrained Coverage

Recall from Definition 1 that a location is said to be covered if it simply lies within the range of a sink-connected node, *irrespective of the number of hops between the node and the sink*. This definition of coverage may be restrictive for delay sensitive applications where a strict constraint is imposed on the number of hops (which is proportional to the delay incurred) within which a packet is expected to reach a sink node for processing. Hence, in this section we will introduce a general notion of coverage by incorporating hop constraint into the definition.

A. Definition and Results

Definition 4: A location $\ell \in \Re_+$ is said to be h**-covered**, $h \geq 0$, if ℓ is within the range of a sink-connected node that is at most h-hops away from a sink node; otherwise ℓ is said to be h***-vacant***.

Let $\mathcal{I}_{V_h} : \Re_+ \to \{0, 1\}$ denote the indicator function that represents whether a location $\ell \in \Re_+$ is left-vacant or not. The fraction of h-vacant region is defined as,

$$v_{\lambda,\beta,h} = \lim_{L\to\infty} \frac{1}{L} \int_0^L \mathcal{I}_{V_h}(\ell) \mathrm{d}\ell. \tag{27}$$

For $h = 0$, a location ℓ is 0-covered if it is simply within the range of a sink node. In this case, the relay nodes do not contribute in extending the coverage. Thus, we are in the framework of a standard coverage process, comprising sink nodes (whose density is $\beta\lambda$) with disks of length $2r$ placed around them. Hence, we readily have $v_{\lambda,\beta,0} = e^{-\beta\lambda 2r}$. However, for $h \geq 1$ the analysis of $v_{\lambda,\beta,h}$ is not straight forward, although some properties can be easily deduced. For instance, it is easy to see that $v_{\lambda,\beta,h}$ is decreasing with h. In fact, we can also obtain a corollary to Theorem 2, yielding a lower bound on $v_{\lambda,\beta,h}$. We formally note the above results.

Lemma 5: The fraction of h-vacant region is decreasing with h, i.e., for $h > h'$ we have $v_{\lambda,\beta,h} \leq v_{\lambda,\beta,h'}$ for all (λ, β). Further, $v_{\lambda,\beta,h} \to v_{\lambda,\beta}$ as $h \to \infty$.

Proof: A location $\ell \in \Re_+$ being h'-covered ($\mathcal{I}_{V_{h'}}(\ell) = 0$) implies that ℓ is h-covered ($\mathcal{I}_{V_h}(\ell) = 0$). However, it is possible for ℓ to be h'-vacant ($\mathcal{I}_{V_{h'}}(\ell) = 1$) while being h-covered ($\mathcal{I}_{V_h}(\ell) = 0$). Thus, we have $\mathcal{I}_{V_h}(\ell) \leq \mathcal{I}_{V_{h'}}(\ell)$, yielding $v_{\lambda,\beta,h} \leq v_{\lambda,\beta,h'}$. Further, since $\mathcal{I}_{V_h}(\ell) \to \mathcal{I}_V(\ell)$ as $h \to \infty$, we have $\lim_{h\to\infty} v_{\lambda,\beta,h} = v_{\lambda,\beta}$. ∎

Corollary 1: Fraction of h-vacant region is lower bounded as follows: $w_{\lambda,\beta,h} \leq v_{\lambda,\beta,h}$, for all (λ, β, h), where

$$w_{\lambda,\beta,h} \quad = \quad e^{-\beta\lambda 2\overline{C}_h}$$

with $2\overline{C}_h$ (analogous to $2\overline{C}$) being the expected length of the *h-coveraged disk* around a sink node, that is obtained by removing all other sink nodes from the network (recall Definition 3).

Proof: The proof is exactly along the lines of the proof of Theorem 2. Details are omitted for brevity. ∎

Remark: We refer to $\overline{C}_h$ as the *h-constrained cluster length* around a sink node, while $\overline{C}$ in (25) is the *unconstrained* cluster length. Unlike $\overline{C}$, it is not easy to derive a general closed-form expression for $\overline{C}_h$. Hence, in the following subsection we propose an approximation for $\overline{C}_h$. The efficacy of our approximation will be numerically demonstrated in Section VII-C.

B. Approximation for $\overline{C}_h$

Without loss of generality we will assume that a sink node is located at the origin (while all other sink nodes are removed). Recall that the location of the relay nodes is represented by a Poisson process Λ of rate $(1-\beta)\lambda$. Alternatively, let $(Z_k : k \geq 1)$ denote the location of the relay nodes; for simplicity, let $Z_0 = 0$. Let C_h $(h \geq 0)$ denote the (random) length of the h-covered disk around the sink at the origin. Note that, $\overline{C}_h = \mathbb{E}[C_h]$. Formally, using the relay locations, C_h can be inductively expressed as follows: $C_0 = r$, and for $h \geq 1$

$$C_h = C_{h-1} + \sup\Big\{Z_k : Z_k \in [C_{h-1} - r, C_{h-1}]\Big\}. \quad (28)$$

Defining, for $h \geq 1$,

$$G_h = \sup\Big\{Z_k : Z_k \in [C_{h-1} - r, C_{h-1}]\Big\}$$

we can alternatively express C_h in terms of the *coverage-increments* $(G_\ell : \ell \geq 1)$ as,

$$C_h \quad = \quad \left(\sum_{\ell=1}^{h} G_\ell\right) + r. \quad (29)$$

See Fig. 5 for an illustration of the above quantities.

Let $\overline{G}_\ell$ denote the expectation of G_ℓ (i.e., $\overline{G}_\ell = \mathbb{E}[G_\ell]$). For instance, $\overline{G}_1$ is given by

$$\overline{G}_1 \quad = \quad r - \frac{1 - e^{-\mu r}}{\mu} \quad (30)$$

where, for simplicity, we let $\mu := (1-\beta)\lambda$ denote the density of relay nodes. To obtain the above expression, note that the distribution function of G_1 is given by, for $x \in [0, r]$,

$$F_{G_1}(x) \quad = \quad \mathbb{P}(G_1 \leq x)$$

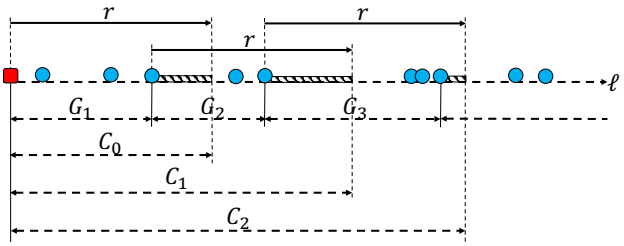

Fig. 5. Illustration of G_ℓ and C_ℓ, $\ell \geq 1$. The hatched segments represent the regions $(C_{\ell-1} + G_\ell, C_\ell + r]$ $(\ell \geq 1)$ that are invariably vacant, given the values of G_ℓ (follows from the definition of G_ℓ).

$$= \quad \mathbb{P}(\Lambda([x, r]) = 0)$$
$$= \quad e^{-\mu(r-x)}.$$

Thus, G_1 has a mass of $e^{-\mu r}$ at 0 and a non-zero density on $[0, r]$ given by

$$f_{G_1}(x) \quad = \quad \mu e^{-\mu(r-x)}. \quad (31)$$

Using the above density function, the expression for $\overline{G}_1$ in (30) can be easily computed. We will also require the second moment of G_1, which is given by

$$\overline{\overline{G}}_1 = \mathbb{E}\left[G_1^2\right] = r^2 - \frac{2\overline{G}_1}{\lambda_R}.$$

In general, for $\ell \geq 1$ the coverage-increment $\overline{G}_\ell$ can be computed as follows:

$$\overline{G}_\ell = \mathbb{E}[G_\ell] = \int_0^r x f_{G_\ell}(x) dx \quad (34)$$

where the density function $f_{G_\ell}(x)$ is given by

$$f_{G_\ell}(x) \quad = \quad \int_0^r f_{G_{\ell-1}}(y) f_{G_\ell|G_{\ell-1}}(x|y) dy \quad (35)$$

with the conditional density $f_{G_\ell|G_{\ell-1}}(x|y)$ given by (see Section C in Supplementary Material for details)

$$f_{G_\ell|G_{\ell-1}}(x|y) = \begin{cases} \mu e^{-\mu(r-x)} & \text{for } x \in [r-y, r] \\ 0 & \text{otherwise.} \end{cases} \quad (36)$$

Thus, computing $\overline{G}_\ell$ involves evaluating the recursive *integral-form* expressions in (34) and (35), which is computationally intensive in general. Hence, in the following, we propose an approximation for $\overline{G}_\ell$ $(\ell \geq 2)$, denoted $\overline{G}_\ell^{(\alpha)}$, where $\alpha \in [0, r]$ is a parameter that can be varied to obtain a range of approximations. The approximation $\overline{G}_\ell^{(\alpha)}$, however, requires knowing all the lower order terms $(\overline{G}_k : k < \ell)$ exactly. Hence, we will later propose a second approximation, denoted $\overline{H}_\ell^{(\alpha)}$, whose computation is completely based on $(\overline{H}_k^{(\alpha)} : k < \ell)$; the form of $\overline{H}_\ell^{(\alpha)}$ is motivated by the structure of $\overline{G}_\ell^{(\alpha)}$. While theoretical guarantees are proved for the first approximation $\overline{G}_\ell^{(\alpha)}$ (see Theorem 3), the efficacy of the second approximation is observed numerically in Section VII-C.

Approximation-1: Let $\overline{G}_1^{(\alpha)} = \overline{G}_1$, and for $\ell \geq 2$, given the lower order terms $(\overline{G}_k : k < \ell)$, the approximation $\overline{G}_\ell^{(\alpha)}$ is computed as in (32), where $\theta_\alpha = (1 + \mu\alpha)e^{-\mu r}$ and $\lfloor x \rfloor$ denotes the smallest integer less than or equal to x. For

$$\overline{G}_{\ell}^{(\alpha)} = \begin{cases} \overline{G}_{\ell-1} - \sum_{k=2,4,\cdots}^{\ell-2} \theta_{\alpha}^{\frac{(\ell-2)-k}{2}} \Big(\mu r \overline{G}_k - \overline{G}_{k-1}\Big) e^{-\mu r} - \theta_{\alpha}^{\left(\frac{\ell}{2}-1\right)} \frac{\mu r^2}{2} e^{-\mu r} & \text{if } \ell \text{ is even} \\ \overline{G}_{\ell-1} - \sum_{k=3,5,\cdots}^{\ell-2} \theta_{\alpha}^{\lfloor \frac{(\ell-2)-k}{2} \rfloor} \Big(\mu r \overline{G}_k - \overline{G}_{k-1}\Big) e^{-\mu r} - \theta_{\alpha}^{\lfloor \frac{\ell}{2}-1 \rfloor} \mu \overline{\overline{G}}_1 e^{-\mu r} & \text{if } \ell \text{ is odd} \end{cases} \tag{32}$$

$$\overline{H}_{\ell}^{(\alpha)} = \begin{cases} \overline{H}_{\ell-1}^{(\alpha)} - \sum_{k=2,4,\cdots}^{\ell-2} \theta_{\alpha}^{\frac{(\ell-2)-k}{2}} \Big(\mu r \overline{H}_k^{(\alpha)} - \overline{H}_{k-1}^{(\alpha)}\Big) e^{-\mu r} - \theta_{\alpha}^{\left(\frac{\ell}{2}-1\right)} \frac{\mu r^2}{2} e^{-\mu r} & \text{if } \ell \text{ is even} \\ \overline{H}_{\ell-1}^{(\alpha)} - \sum_{k=3,5,\cdots}^{\ell-2} \theta_{\alpha}^{\lfloor \frac{(\ell-2)-k}{2} \rfloor} \Big(\mu r \overline{H}_k^{(\alpha)} - \overline{H}_{k-1}^{(\alpha)}\Big) e^{-\mu r} - \theta_{\alpha}^{\lfloor \frac{\ell}{2}-1 \rfloor} \mu \overline{\overline{G}}_1 e^{-\mu r} & \text{if } \ell \text{ is odd} \end{cases} \tag{33}$$

instance, evaluating (32) for $\ell = 2$ and $\ell = 3$ we obtain, respectively,

$$\overline{G}_2^{(\alpha)} = \overline{G}_1 - \frac{\mu r^2}{2} e^{-\mu r} \tag{37}$$

$$\overline{G}_3^{(\alpha)} = \overline{G}_2 - \mu \overline{\overline{G}}_1 e^{-\mu r}. \tag{38}$$

The higher order terms can be evaluated similarly. Note that the expressions for $\overline{G}_2^{(\alpha)}$ and $\overline{G}_3^{(\alpha)}$ does not depend on the parameter α; however, the higher order terms are, in general, functions of α.

In the following theorem we show that $G_{\ell}^{(\alpha)}$ evaluated at the extreme values of α (i.e., $\alpha = r$ and $\alpha = 0$, respectively) serve as lower and upper bounds (respectively) for $\overline{G}_{\ell}$. Further, a range of approximations, with values lying between the upper and lower bound values, are obtained by varying α.

Theorem 3: For $\ell \geq 1$, we have

$$\overline{G}_{\ell}^{(r)} \leq \overline{G}_{\ell} \leq \overline{G}_{\ell}^{(0)}. \tag{39}$$

Also, for $\alpha \in [0, r]$, we have

$$\overline{G}_{\ell}^{(r)} \leq \overline{G}_{\ell}^{(\alpha)} \leq \overline{G}_{\ell}^{(0)}. \tag{40}$$

Proof: Available in Supplementary Material. ∎

The following corollary is a simple consequence of the above theorem.

Corollary 2: For $h \geq 1$, we have

$$\left(\sum_{\ell=1}^{h} \overline{G}_{\ell}^{(r)}\right) + r \;\leq\; \overline{C}_h \;\leq\; \left(\sum_{\ell=1}^{h} \overline{G}_{\ell}^{(0)}\right) + r. \tag{41}$$

Proof: Follows from (29) and Theorem 3. ∎

Approximation-2: Motivated by the form of the approximation $\overline{G}_{\ell}^{(\alpha)}$ in (32), we propose a second approximation $\overline{H}_{\ell}^{(\alpha)}$, where $\overline{H}_1^{(\alpha)} = \overline{G}_1^{(\alpha)}$, while for $\ell \geq 2$ the expression for $\overline{H}_{\ell}^{(\alpha)}$ is as in (33). Note that, the computation of $\overline{H}_{\ell}^{(\alpha)}$ is completely *stand-alone*, in the sense that $\overline{H}_{\ell}^{(\alpha)}$ can be evaluated using only the lower order approximations $\{\overline{H}_k^{(\alpha)} : k \leq \ell - 1\}$. This is in contrast to $\overline{G}_{\ell}^{(\alpha)}$, whose computation requires the knowledge to the true expectations $\overline{G}_k$ (of G_k) for all $k \leq \ell - 1$. Thus, $\overline{H}_{\ell}^{(\alpha)}$ is a practically computable approximation. Although we do not have results analogous to that for $\overline{G}_{\ell}^{(\alpha)}$ in Theorem 3, numerically (in Section VII-C) we find that $\overline{H}_{\ell}^{(\alpha)}$ also yields a range of approximations for $\overline{G}_{\ell}$ as α is varied, including upper and lower bounds, respectively, for $\alpha = 0$ and $\alpha = r$. In fact, motivated by our numerical observations in Section VII-C we conjecture the following.

Conjecture 2: For $\ell \geq 1$, we conjecture that

$$\overline{H}_{\ell}^{(r)} \leq \overline{G}_{\ell}^{(r)} \leq \overline{G}_{\ell} \leq \overline{G}_{\ell}^{(0)} \leq \overline{H}_{\ell}^{(0)}.$$

Finally, given $\overline{H}_{\ell}^{(\alpha)}$, an approximation to the cluster length $\overline{C}_h$ can be naturally written as, for $\alpha \in [0, r]$,

$$\overline{C}_h^{(\alpha)} := \left(\sum_{\ell=1}^{h} \overline{H}_{\ell}^{(\alpha)}\right) + r. \tag{42}$$

Again, numerically we observe that the above approximation, evaluated at $\alpha = 0$ and $\alpha = r$, respectively, yields upper and lower bounds for $\overline{C}_h$. Furthermore, we find that $\overline{C}_h^{(\alpha)}$, evaluated at $\alpha = 0.5$, in fact, serves as a very good approximation for the true cluster length, $\overline{C}_h$, at least for the considered numerical setting; details are discussed in Section VII-C.

VII. Numerical & Simulation Work

Without loss of generality, we assume a normalized range of $r = 1$. Thus, the node density λ is in the units of number-of-nodes per range. Also, we fix the cost of a relay node to $c_R = 1$ unit. In the following subsections we first (in Section VII-A) study the properties of the average vacancy, while also drawing a comparison with the proposed upper and lower bounds. In Section VII-B we investigate the network optimization problem proposed in (4). Finally, in Section VII-C we evaluate hop-constrained coverage along with the proposed approximations for the average cluster length.

A. Average Vacancy, Upper and Lower Bounds

In Fig. 6(a) we plot the average vacancy $v_{\lambda,\beta}$ as a function of λ for different values of β. As shown in Lemma 3 (a), we see that $v_{\lambda,\beta}$ is a decreasing function of λ for any given β; similarly, for a given λ, $v_{\lambda,\beta}$ decreases with β. Also shown in Fig. 6(a) are the upper-bound ($u_{\lambda,\beta}$ vs. λ) and lower-bound curves ($w_{\lambda,\beta}$ vs. λ), for different values of β.

We observe that the upper-bound curves are a good approximation for the exact vacancy curves for small values of β, while the quality of the approximation deteriorates as β increases. This is because, as β increases more connected components contain sink nodes so that the region of length r preceding the connected components are actually covered while they remain left-vacant in the upper bound process, thus

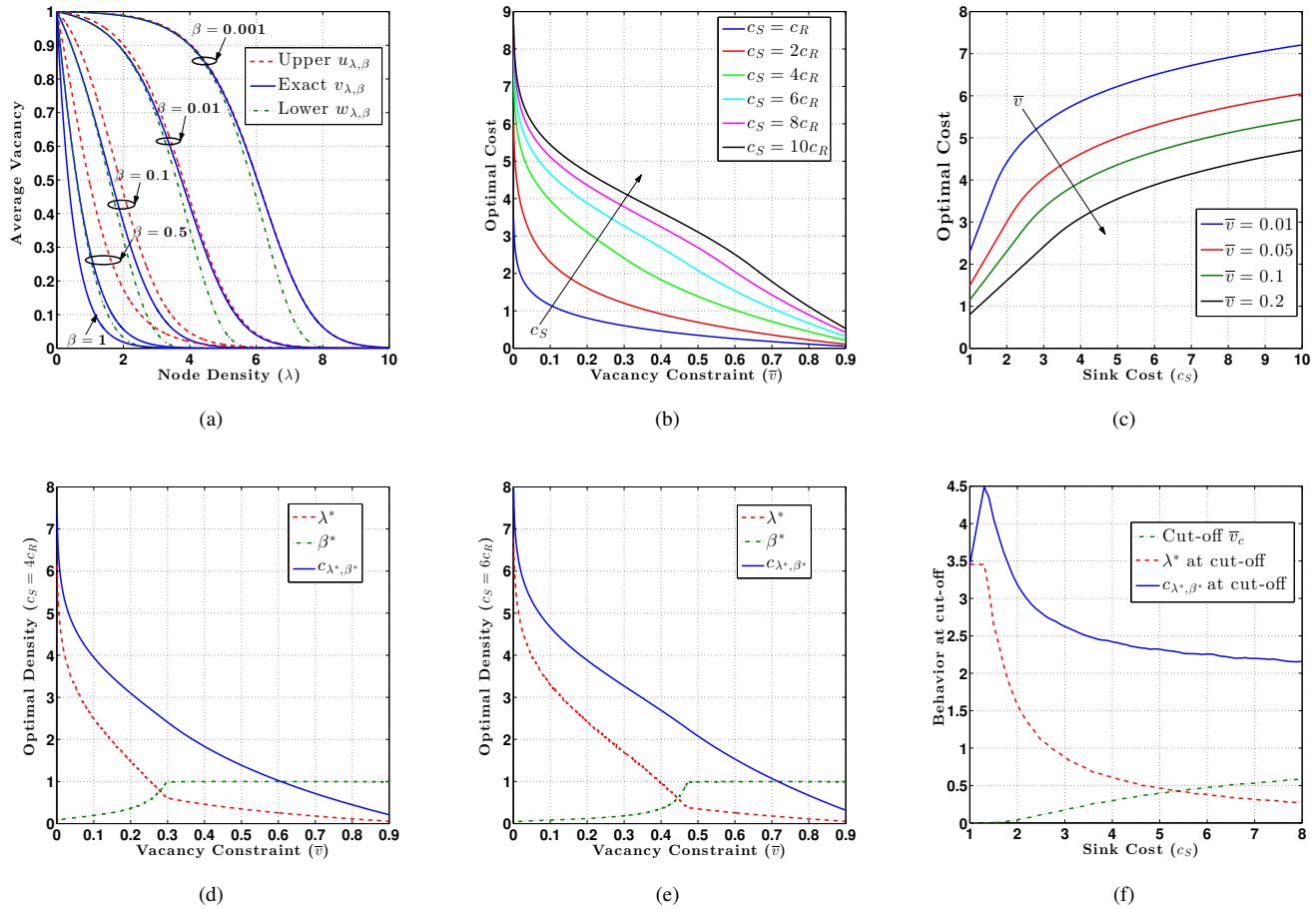

Fig. 6. (a) Average vacancy as a function of λ for different values of β; the respective upper and lower bound curves are also shown. (b) Optimal cost vs. vacancy constraint for different values of sink-cost. (c) Optimal cost vs. sink-cost curves for different values of vacancy constraint ($\overline{v}$). (d) and (e): Optimal node density as a function of the vacancy constraint for $c_s = 4c_R$ and $c_s = 6c_R$, respectively. (f) Behavior at cut-off as a function of the sink-cost.

increasing the contribution of the term that was left out in order to obtain the bound.

The lower bound curves should be understood as follows (although these appear to be a good approximation for the exact curves for larger values of β). For a given node density λ, observe that the difference between $v_{\lambda,\beta}$ and $w_{\lambda,\beta}$ increases as β increases. For instance, fixing $\lambda = 3$ we see that the difference, $v_{\lambda,\beta} - w_{\lambda,\beta}$, increases as β increases from $\beta = 0.001$ to $\beta = 0.1$ (curves corresponding to $\beta = 0.5$ have already saturated to 0). Hence, the lower bound is actually a good approximation for the average vacancy for smaller values of β. This is because, smaller β implies a larger distance of separation between successive sink nodes, so that the probability of adjacent coverage disks overlapping is small. Thus, essentially it appears as if i.i.d. coverage disks are placed around each sink node. Hence, the original dependent-disk model approaches the independent-disk model as β decreases, so that the respective average vacancies are comparable. However, the above effect gets nullified as λ increases with β remaining fixed. This observation can be made from Fig. 6(a) where we see that, for a fixed β, the lower-bound's approximation deteriorates as λ increases. This is essentially due to the increase in the length of the coverage disk as λ increases. As a result, the probability that the adjacent disks overlap increases, thus increasing the dependency in the model.

B. Network Optimization

Recall the network optimization problem in (4) along with the simplified formulation in (23). We compute the optimal cost by solving the simplified formulation since it is of lower complexity than the original problem. The approach we implement is based on discretizing the problem. Specifically, for a given c_S and $\overline{v}$, using (24) we first compute $c(\beta)$ by varying β from 0.001 to 1 in steps of 0.001. The minimizer β^* along with the optimal cost $c_{\lambda^*,\beta^*} = c(\beta^*)$ are then identified, where $\lambda^* = \lambda(\beta^*)$ is computed using (22). The process is repeated for different values of c_S and $\overline{v}$.

In Fig. 6(b) we plot the optimal network cost, c_{λ^*,β^*}, as a function of the vacancy constraint, $\overline{v}$. The curves are shown for different values of sink to relay cost ratios (c_S/c_R), where recall that we have normalized the relay cost to 1 unit. Alternatively, in Fig. 6(c) we depict the optimal cost as a function of the sink cost c_S for different values of vacancy constraint $\overline{v}$. From Fig. 6(c) we observe that the optimal cost behaves as a concave function of c_S, for any $\overline{v}$. As a result we find that, in the *high-c_S regime* a small reduction in c_S does not significantly reduce the network cost; while in the *low-c_S regime*, an equivalent reduction in c_S can yield noticeable cost gains. For instance, fixing $\overline{v} = 0.1$, (from both Fig. 6(b) and 6(c)) we see that the network cost reduces by only 6% (from 5.4 to 5.1) when c_S reduces from $10c_R$ to $8c_R$, while it is

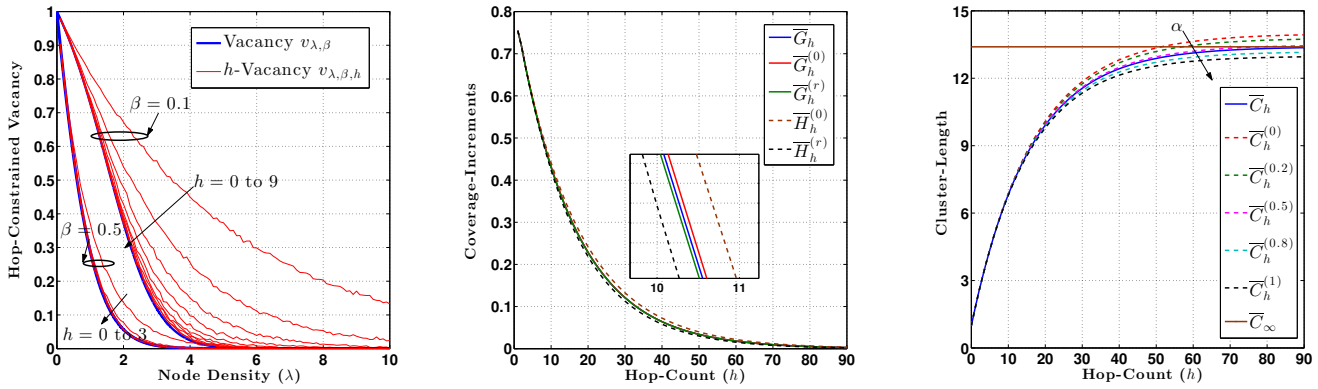

(a) (b) (c)

Fig. 7. (a) Hop-constrained vacancy as a function of node density. (b) Coverage-increments vs. hop-count. (c) Cluster-length vs. hop-count.

more than 40% (4 to 2.3) for $c_S = 4c_R$ to $2c_R$ reduction. The above behavior can be understood as follows. When the sink nodes are expensive (*high-c_S regime*), optimal network design would comprise only a small fraction of sink nodes, so that a small reduction in sink cost would not greatly reduce the network cost. On the other hand, in the *low-c_S regime* where the sink nodes are inexpensive, the network would almost entirely consist of sink nodes; as a result, a small reduction in sink cost would result in a large savings in the network cost.

Summarizing the above observations we conclude that, when the backhaul is inexpensive (so that the cost of deploying a sink node is low), noticeable gains can be achieved by optimizing the backhaul design[5]; Otherwise (i.e., when the backhaul is expensive), incremental optimization of the backhaul is not necessary as it yields only marginal gains.

Further insights into the structure of the optimal network can be gained through Fig. 6(d) and 6(e), where (for $c_S = 4c_R$ and $c_S = 6c_R$, respectively) we have shown how λ^* and β^* (optimal node density and sink probability) varies with the vacancy constraint $\overline{v}$. From these figures we observe that there is a cut-off value of $\overline{v}$, denoted $\overline{v}_c$, beyond which $\beta^* = 1$. Thus, if a vacancy of more than the cut-off is tolerable then the optimal network design comprises only sink nodes. The respective cut-offs in Fig. 6(d) and 6(e) are (approximately) $\overline{v}_c = 0.3$ and $\overline{v}_c = 4.7$. Hence, there is a shift in the cut-off towards the right as the cost of the sink nodes increases. This is expected because as the sink-node's cost increases it is important to be cautious about using more sink nodes in the network. On the other hand, if the vacancy constraint is less than the cut-off, the optimal network comprises both sink and relay nodes. In fact, the fraction of sink nodes required reduces as the vacancy constraint is lowered. For instance, from Fig. 6(d) we see that $\beta^* = 0.37$ when $\overline{v} = 0.2$ as compared to $\beta^* = 0.19$ for $\overline{v} = 0.1$. However, the respective λ^* are 1.5 and 2.5 so that the network cost is much lower when $\overline{v} = 0.2$ although the corresponding β^* is more. Similar observations can be made from Fig. 6(e).

Accumulating the results in Fig. 6(d) and 6(e) (along with the result corresponding to other values c_S), in Fig. 6(f) we plot the cut-off value $\overline{v}_c$ as a function of c_S. Also shown in the figure are the optimal node density and optimal cost at cut-off (note that $\beta^* = 1$ at cut-off). From Fig. 6(f) it is interesting to observe that there is a threshold on the sink cost of $c_S = 1.3$ below which $\overline{v}_c$ is close to 0, implying that an all-infrastructure design is optimal in this regime. Further, we observe that λ^* remains constant until $c_S = 1.3$. As a result, the optimal cost increases linearly in c_S until the threshold of 1.3. However, beyond $c_S = 1.3$ we observe that $\overline{v}_c$ steadily increases, while both λ^* and c_{λ^*,β^*} decreases with c_S.

The behavior in Fig. 6(f) can be understood as follows. Let us first fix a vacancy constraint $\overline{v}_0$ close to zero. Now, when $c_S = c_R$, since the sink and relay nodes are identical in terms of cost, it is optimal to go for an all-sink network design (so that $\beta^* = 1$) to achieve the required vacancy constraint of $\overline{v}_0$; let us denote the corresponding value of λ^* as λ_0 (from Fig. 6(f) we identify that $\lambda_0 = 3.45$). For simplicity, define $\beta_0 = 1$. Now, as c_S increases, the vacancy constraint of $\overline{v}_0$ can be maintained by

- either fixing (λ, β) at (λ_0, β_0) in which case the cost $c_{\lambda,\beta} = \lambda_0\beta_0 c_S$ increases linearly with c_S (in Fig. 6(f), see the increasing portion of the curve c_{λ^*,β^*}), or
- by optimally choosing a $\lambda > \lambda_0$ and $\beta < \beta_0$ (so that relay nodes are introduced at the expense of increased node density) in which case the cost $c_{\lambda,\beta}$ decreases with c_S (in Fig. 6(f), imagine the decreasing portion of the curve c_{λ^*,β^*} extended to the range $c_S = 1$ to 1.3).

The respective increasing and decreasing cost functions intersect at $c_S = 1.3$. Thus, the former option yields a lower cost until $c_S = 1.3$ (hence, $\overline{v}_c = \overline{v}_0 \approx 0$ in this range since $\beta^* = \beta_0$), while the latter option is optimal beyond $c_S = 1.3$ (as a result, $\overline{v}_c$ starts increasing since $\beta^* < 1$ in this regime).

C. Hop-Constrained Vacancy

We resort to simulations to compute the hop-constrained vacancies, $v_{\lambda,\beta,h}$. These results are reported in Fig. 7(a) where, for $\beta = 0.1$ and $\beta = 0.5$, $v_{\lambda,\beta,h}$ are shown as functions of λ for different values of h (the arrowed lines in Fig. 7(a) indicates the direction along which h increases). Also shown in the figure are corresponding vacancy curves, $v_{\lambda,\beta}$. As expected we observe that as h increases the hop-constrained curves, $v_{\lambda,\beta,h}$, converge to the respective vacancy curves, $v_{\lambda,\beta}$.

[5]Backhaul design optimization can be accomplished by allocating additional resources toward finding even cheaper hardware and operating costs associated with the sink node.

However, the value of h for which good approximation to $v_{\lambda,\beta}$ is achieved is larger for $\beta = 0.1$ than for $\beta = 0.5$ ($h = 9$ and $h = 3$, respectively). This is because, when $\beta = 0.1$ the successive sink nodes are farther apart so that a larger value of h is required to completely cover the sink-containing busy periods (which are always completely covered when h is unconstrained).

In Fig. 7(b) and 7(c) we demonstrate the efficiency of the approximations proposed in Section VI-B; these plots correspond to $\mu = 4$ (recall that μ denotes the density of relay nodes). First, in Fig. 7(b) we depict coverage-increments $\overline{G}_h$ as a function of the hop-count h. Also shown are the approximations $\overline{G}_h^{(\alpha)}$ and $\overline{H}_h^{(\alpha)}$ for $\alpha = 0$ and $\alpha = r$. Recall from Theorem 3 that $\overline{G}_h^{(\alpha)}$, evaluated at $\alpha = 0$ and $\alpha = r$, respectively yield upper and lower bounds for the true coverage-increment $\overline{G}_h$. We find that the upper and lower bounds coincide so well that these plots are practically indistinguishable from the true $\overline{G}_h$ curve; we hence provide an inset in Fig. 7(b) so that the all the curves are distinctly emphasized. From Fig. 7(b) we also find that $\overline{H}_h^{(\alpha)}$, evaluated at $\alpha = 0$ and $\alpha = r$, yield good upper and lower bound approximations for $\overline{G}_h$; this observation is in line with our conjecture in Section VI-B (recall Conjecture VI-B).

In Fig. 7(c) we plot the average cluster-length, $\overline{C}_h$, along with the approximations $\overline{C}_h^{(\alpha)}$ in (42) for different values of α. The horizontal line in Fig. 7(c) corresponds to the unconstrained length of the cluster $\overline{C}_\infty = \overline{C}$, whose expression is as given in (25); note that $\overline{C}_h$ converges to $\overline{C}_\infty$ as h increases. While $\overline{C}_h^{(\alpha)}$, for $\alpha = 0$ and $\alpha = r$, serves as upper and lower bounds (respectively) for $\overline{C}_h$, a range of approximations that lie between these two extremes are obtained by varying α; in fact, $\overline{C}_h^{(\alpha)}$ decreases with α. Interestingly, we find that $\overline{C}_h^{(\alpha)}$, evaluated at $\alpha = 0.5$, yields a very good approximation for the true cluster length $\overline{C}_h$.

Remark: Regarding computational complexity, we would like to note that determining exact cluster length $\overline{C}_h$ involves computing the (recursive) *integral expressions* in (34) and (35), which is intensive in general. In contrast, the approximation $\overline{C}_h^{(\alpha)}$ requires computing the simple (recursive) *linear expressions* in (33), which involves only additions and multiplications. Thus, the approximation is far easier to compute. However, we would like to note that determining the value of the approximation parameter α that achieves the best cluster-length approximation (i.e., $\overline{C}_h^{(\alpha)} \approx \overline{C}_h$) is not easy in general (and is out of our current scope). This is primarily because of the integral and the linear form expressions involved in the computation of $\overline{C}_h$ and $\overline{C}_h^{(\alpha)}$, that prevents us from establishing any form of relation between the two quantities.

Finally, in Fig. 8 we plot optimal cost as a function of hop constraint ($\overline{h}$) that is obtained by solving (via simulation and numerical analysis) the following generalization of the network optimization problem in (4):

$$\begin{array}{ll} \text{Minimize}_{(\lambda,\beta)} & c_{\lambda,\beta} \\ \text{Subject to} & v_{\lambda,\beta,h} \leq \overline{v} \text{ and } h \leq \overline{h}. \end{array} \tag{43}$$

In the above formulation, $\overline{v}$ denotes the vacancy constraint (as before), while $\overline{h}$ is the hop constraint that could model delay constraints in applications that are sensitive to delays. The plot in Fig. 8 corresponds to $\overline{v} = 0.1$, while $\overline{h}$ is varied from 0 to 10; $\overline{h} = \infty$ simply corresponds to the unconstrained problem in (4). The individual curves in Fig. 8 correspond to different values of the sink cost c_S. As in the case of unconstrained optimization, we note that both the constraints in (43) are met at the optimal (which follows from the form of $v_{\lambda,\beta,h}$ in Fig. 7(a)).

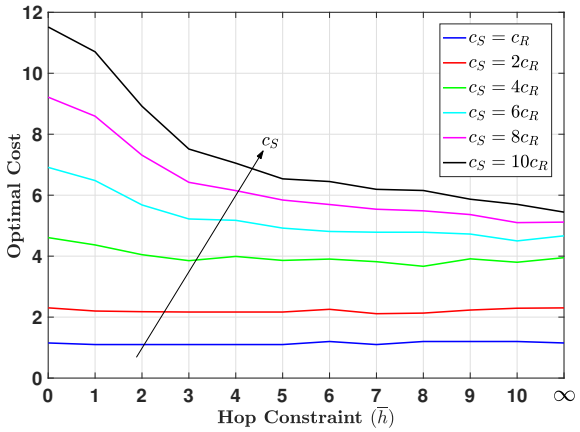

Fig. 8. Optimal cost vs. hop constraint ($\overline{h}$) for vacancy constraint $\overline{v} = 0.1$.

From Fig. 8 we observe that the optimal cost does not vary with $\overline{h}$ when the sink cost is comparable with that of relay's (see the plots corresponding to $c_S = c_R$ and $c_S = 2c_R$). This is essentially because, whenever $c_S \approx c_R$, it is optimal to adopt an all-infrastructure design (i.e., $\beta^* = 1$), in which case a location that is covered is also h-covered for any $h \geq 0$. As a result, the hop constraint in (43) would be rendered redundant. In contrast, when the sinks are much more expensive than relays, relaxing the hop constraint yields significant gains in terms of cost reduction. For instance, when $c_S = 10c_R$, from Fig. 8 we see that the optimal cost reduces (approximately) from 11.5 to 7 when $\overline{h}$ is relaxed from 0 to 4, respectively. This is because, higher hop-constraints can be met with reduced sink and/or relay densities, thus yielding lower costs.

In summary, an infrastructure-based design (comprising both sink and relays) is recommended whenever the application under consideration (for which the network is being planned) is delay-tolerant.

VIII. Conclusion

Motivated by the possibility of installed wireless networks that would be readily available for deploying IoT applications, we have studied a new class of coverage problems arising in one-dimensional wireless networks comprising infrastructure nodes whose coverage is extended by deploying some relay nodes. A point is covered even if it is in range of a relay node, which, in turn, is connected by a multihop path to an infrastructure node.

For the proposed model, our theoretical contribution includes deriving a closed-form expression for average vacancy (expression (19)). This result is a generalization of the classical expression for vacancy (i.e., $v_{\lambda,1} = e^{-2\lambda r}$) known for traditional coverage processes. In addition to the above result, we also derived bounds on the average vacancy. First, a simple upper bound was obtained by introducing the notion

of left-vacancy (Lemma 1). Then, via. an interesting coupling argument we showed that the average vacancy created in an alternate independent-disk model serves as a lower bound for the vacancy in the proposed model (Theorem 2). We also explored the problem of minimizing the average deployment cost of the network subject to a constraint on the average vacancy. We established interesting quasi-convexity results for the proposed formulation (Lemma 3 and discussions therein).

On the numerical front, we first conducted experiments to determine the efficacy of the theoretical bounds (Fig. 6(a)); specifically, we found that the upper bound (respectively lower bound) serves as a good approximation for average vacancy at low (respectively high) sink densities. For the network optimization problem we find that there exists a threshold on the vacancy constraint such that below the threshold an infrastructure-based design (comprising both sink and relay nodes) is optimal while above the threshold an all-infrastructure design (comprising only sink nodes) suffices (Fig. 6(d)-(f)). Finally, we introduced a generalized notion of hop-constrained coverage; easy-to-compute approximations for the cluster-lengths (i.e., length of the coverage region around a sink node) were proposed (expression (33)), whose efficacy was validated numerically. Through a hop-constrained cost optimization framework we demonstrate the gains that can be achieved by the infrastructure-based design, particular when the network application can tolerate some delay (Fig. 8).

ACKNOWLEDGEMENT

The authors would like to thank the editor and the anonymous reviewers for their valuable comments and suggestions.

REFERENCES

[1] K. P. Naveen and A. Kumar, "Coverage Properties of One-Dimensional Infrastructure-Based Wireless Networks," in *Proceedings of the 19th ACM International Conference on Modeling, Analysis and Simulation of Wireless and Mobile Systems*, ser. MSWiM '16. New York, NY, USA: ACM, 2016, pp. 348–357.

[2] R. Gravina, P. Alinia, H. Ghasemzadeh, and G. Fortino, "Multi-Sensor Fusion in Body Sensor Networks: State-of-the-Art and Research Challenges," *Information Fusion*, vol. 35, pp. 68 – 80, 2017.

[3] P. Gope and T. Hwang, "BSN-Care: A Secure IoT-Based Modern Healthcare System Using Body Sensor Network," *IEEE Sensors Journal*, vol. 16, no. 5, pp. 1368–1376, March 2016.

[4] Erricsson, "5G Radio Access," *White Paper*, April 2016.

[5] A. Bhattacharya and A. Kumar, "An Approximation to the QoS Aware Throughput Region of a Tree Network Under IEEE 802.15.4 CSMA/CA with Application to Wireless Sensor Network Design," *Ad Hoc Networks*, vol. 33, pp. 35 – 54, 2015.

[6] P. Hall, *Introduction to the Theory of Coverage Processes*, ser. Wiley Series in Probability and Mathematical Statistics. NY: Wiley, 1988.

[7] J. G. Andrews, F. Baccelli, and R. K. Ganti, "A Tractable Approach to Coverage and Rate in Cellular Networks," *IEEE Transactions on Communications*, vol. 59, no. 11, pp. 3122–3134, November 2011.

[8] H. S. Dhillon, R. K. Ganti, and J. G. Andrews, "A Tractable Framework for Coverage and Outage in Heterogeneous Cellular Networks," in *ITA 11', Information Theory and Applications Workshop*, Feb 2011.

[9] F. Baccelli and B. Bartlomiej, "On a Coverage Process Ranging from the Boolean Model to the Poisson-Voronoi Tessellation with Applications to Wireless Communications," *Advances in Applied Probability*, vol. 33, no. 2, pp. 293–323, 2001.

[10] P. Gupta and P. R. Kumar, *Critical Power for Asymptotic Connectivity in Wireless Networks*. Boston, MA: Birkhäuser Boston, 1999, ch. Stochastic Analysis, Control, Optimization and Applications: A Volume in Honor of W.H. Fleming, pp. 547–566.

[11] R. S. Ojha, G. Kannan, S. N. Merchant, and U. B. Desai, "On Optimal Transmission Range for Multihop Cellular Networks," in *GLOBECOM 08', IEEE Global Telecommunications Conference*, Nov 2008.

[12] P. Santi, "The Critical Transmitting Range for Connectivity in Mobile Ad Hoc Networks," *IEEE Transactions on Mobile Computing*, vol. 4, no. 3, pp. 310–317, May 2005.

[13] D. Miorandi, E. Altman, and G. Alfano, "The Impact of Channel Randomness on Coverage and Connectivity of Ad Hoc and Sensor Networks," *IEEE Transactions on Wireless Communications*, vol. 7, no. 3, pp. 1062–1072, March 2008.

[14] C. Bettstetter and C. Hartmann, "Connectivity of Wireless Multihop Networks in a Shadow Fading Environment," *Wireless Networks*, vol. 11, no. 5, pp. 571–579, September 2005.

[15] X. Gan, Z. Zhang, L. Fu, X. Wu, and X. Wang, "Unraveling Impact of Critical Sensing Range on Mobile Camera Sensor Networks," *IEEE Transactions on Mobile Computing*, pp. 1–15, 2019.

[16] M. Desai and D. Manjunath, "On the Connectivity in Finite Ad Hoc Networks," *IEEE Comms. Letters*, vol. 6, no. 10, pp. 437–439, Oct 2002.

[17] D. Miorandi and E. Altman, "Connectivity in One-Dimensional Ad Hoc Networks: A Queueing Theoretical Approach," *Wireless Networks*, vol. 12, no. 5, pp. 573–587, 2006.

[18] O. Dousse, P. Thiran, and M. Hasler, "Connectivity in Ad-Hoc and Hybrid Networks," in *INFOCOM 02', Twenty-First Annual Joint Conference of the IEEE Computer and Communications Societies*, 2002.

[19] S. I. Sou, "A Power-Saving Model for Roadside Unit Deployment in Vehicular Networks," *IEEE Communications Letters*, vol. 14, no. 7, pp. 623–625, July 2010.

[20] S. C. Ng, G. Mao, and B. D. O. Anderson, "On the Properties of One-Dimensional Infrastructure-Based Wireless Multi-Hop Networks," *IEEE Transactions on Wireless Communications*, vol. 11, no. 7, pp. 2606–2615, July 2012.

[21] W. Zhang, Y. Chen, Y. Yang, X. Wang, Y. Zhang, X. Hong, and G. Mao, "Multi-Hop Connectivity Probability in Infrastructure-Based Vehicular Net- works," *IEEE Journal on Selected Areas in Comm- unications*, vol. 30, no. 4, pp. 740–747, May 2012.

[22] J. G. Andrews, F. Baccelli, and R. K. Ganti, "A Tractable Approach to Coverage and Rate in Cellular Networks," *IEEE Transactions on Communications*, vol. 59, no. 11, pp. 3122–3134, November 2011.

[23] J. G. Andrews, R. K. Ganti, M. Haenggi, N. Jindal, and S. Weber, "A Primer on Spatial Modeling and Analysis in Wireless Networks," *IEEE Communications Magazine*, vol. 48, no. 11, pp. 156–163, Nov 2010.

[24] R. W. Wolff, *Stochastic Modeling and the Theory of Queues*, ser. Prentice-Hall International Series in Industrial and Systems Engineering. Englewood Cliffs, N.J. Prentice Hall, 1989.

[25] D. Cox, *Renewal Theory*, ser. Methuen's Monographs on Applied Probability and Statistics. Methuen, 1970.

[26] S. Boyd and L. Vandenberghe, *Convex Optimization*. New York, NY, USA: Cambridge University Press, 2004.

[27] G. Lindgren, *Stationary Stochastic Processes: Theory and Applications*, ser. Texts in Statistical Science. Chapman and Hall, 2012.

K. P. Naveen received the B.E. degree in ECE from the Visveswaraiah Technological University, Belgaum, in 2005, and the Ph.D. degree from the Department of Electrical Communication Engineering, Indian Institute of Science (IISc), Bangalore, in 2013. His work experience includes Sci/Engg. SC, ISRO Satellite Centre, Bangalore (Jan 2006 - July 2007), Post-doctoral Fellow, INRIA Saclay, France (Jan 2014 - Dec 2015), and INSPIRE Faculty, Dept. of Electrical Engineering, Indian Institute of Technology (IIT) Madras (Jan 2016 - July 2017). Since August 2017 he is with the Dept. of Electrical Engineering at IIT Tirupati. His research interests include modeling and performance analysis of wireless networks, network economics, games and optimal control.

Anurag Kumar (B.Tech., Indian Institute of Technology (IIT) Kanpur; Ph.D., Cornell University, both in Electrical Engineering) was with Bell Labs, Holmdel, N.J., for over 6 years. Since then he has been on the faculty of the ECE Department at the Indian Institute of Science (IISc), Bangalore; he is at present the Director of the Institute. His area of research is communication networking, and he has recently focused primarily on wireless networking. He is a Fellow of the IEEE, the Indian National Science Academy (INSA), the Indian National Academy of Engineering (INAE), and the Indian Academy of Sciences (IASc). He was an associate editor of IEEE/ACM Transactions on Networking, and of IEEE Communications Surveys and Tutorials.

SUPPLEMENTARY MATERIAL

A. Expressions for p, Q and $\overline{Q}$

Recall that $p = \mathbb{P}(\mathcal{S}_k^c)$, $Q = \mathbb{E}[B_k|\mathcal{S}_k^c]$, and $\overline{Q} = \mathbb{E}[B_k|\mathcal{S}_k]$, where $\mathcal{S}_k$ is the event that the k-th connected component contains a sink, and $\mathcal{S}_k^c$ is the complement of $\mathcal{S}_k$. Thus, p is the probability that the k-th connected component does not contain a sink, while Q (respectively, $\overline{Q}$) is the expected length of the k-th busy period conditioned on $\mathcal{S}_k^c$ (respectively, $\mathcal{S}_k$).

Let N_k denote the number of nodes in the k-th busy period. Note that N_k is a geometric random variable with success probability $e^{-\lambda r}$ (which is the probability that the region of length r towards the right of the N_k-th node is empty, thus terminating the busy period). Conditioning on $(N_k = n)$ we can write

$$\begin{aligned} p &= \sum_{n=1}^{\infty} \mathbb{P}(N_k = n)\ \mathbb{P}(\mathcal{S}_k^c|N_k = n) \\ &= \sum_{n=1}^{\infty} (1-e^{-\lambda r})^{n-1}\ e^{-\lambda r}\ (1-\beta)^n \\ &= (1-\beta)e^{-\lambda r} \sum_{n=1}^{\infty} [(1-e^{-\lambda r})(1-\beta)]^{n-1} \\ &= \frac{(1-\beta)e^{-\lambda r}}{\beta + e^{-\lambda r} - \beta e^{-\lambda r}}. \end{aligned} \tag{44}$$

Computation of Q is along similar lines, although it is more involved. Denoting $Q_n := \mathbb{E}[B_k|\mathcal{S}_k^c, N = n]$, we have

$$\begin{aligned} Q &= \sum_{n=1}^{\infty} \mathbb{P}(N_k = n|\mathcal{S}_k^c) Q_n \\ &= \frac{1}{p} \sum_{n=1}^{\infty} \mathbb{P}(N_k = n)\mathbb{P}(\mathcal{S}_k^c|N_k = n) Q_n \end{aligned} \tag{45}$$

Now, let $D_i, i = 1, \cdots N_k - 1$, denote the distance between the i-th and $(i+1)$-th node in the k-th connected component. Note that, $\{D_i\}$ are i.i.d. exponentially distributed random variables of rate λ. Hence, we can write

$$Q_n = \mathbb{E}\left[\sum_{i=1}^{N_k - 1} D_i + r \middle| \mathcal{S}_k^c, N_k = n \right] = (n-1)\overline{D} + r \tag{46}$$

where

$$\overline{D} = \mathbb{E}\Big[D_1 \Big| D_1 \le r \Big] = \frac{(1 - e^{-\lambda r} - \lambda r e^{-\lambda r})}{\lambda(1 - e^{-\lambda r})}. \tag{47}$$

Substituting (46) in (45) and simplifying we obtain

$$\begin{aligned} Q &= \frac{p(1-e^{-\lambda r})}{e^{-\lambda r}} \overline{D} + r \\ &= \frac{p(1-e^{-\lambda r})}{\lambda e^{-\lambda r}} + (1-p)r. \end{aligned}$$

Recalling the expression for $\mathbb{E}[B_k]$ from (6), we have

$$Q = p\mathbb{E}[B_k] + (1-p)r. \tag{48}$$

Finally, $\overline{Q}$ can be obtained using the total expectation identity:

$$\begin{aligned} \mathbb{E}[B_k] &= \mathbb{P}(\mathcal{S}_k)\mathbb{E}[B_k|\mathcal{S}_k] + \mathbb{P}(\mathcal{S}_k^c)\mathbb{E}[B_k|\mathcal{S}_k^c] \\ &= (1-p)\overline{Q} + pQ \end{aligned}$$

so that we have

$$\overline{Q} = \frac{\mathbb{E}[B_k] - pQ}{(1-p)}. \tag{49}$$

Discussion: Since $\mathbb{E}[B_k] \ge r$, from (48) we see that $Q \le \mathbb{E}[B_k]$, which implies that $\overline{Q} \ge \mathbb{E}[B_k]$. Thus, the busy periods not containing sink nodes are shorter in length than the busy periods containing sink nodes. Indeed, as $\beta \to 1$, from (44) we see that $p \to 0$, yielding $Q \to r$ and $\overline{Q} \to \mathbb{E}[B_k]$. Thus, as β approaches 1, the busy periods not containing sink nodes are essentially the ones consisting of an isolated relay node (thus, $Q \approx r$), while the regular busy periods always contain sink nodes (so that, $\overline{Q} \approx \mathbb{E}[B_k]$).

B. Proof of Lemma 3

Proof of Part (a): The partial derivatives of $v_{\lambda,\beta}$ w.r.t λ and β, respectively, are given by

$$\begin{aligned} \frac{\partial v_{\lambda,\beta}}{\partial \lambda} &= \frac{-2\beta r e^{\lambda r}}{\Big(1 - \beta + \beta e^{\lambda r}\Big)^3} \\ \frac{\partial v_{\lambda,\beta}}{\partial \beta} &= \frac{-2\Big(e^{\lambda r} - 1\Big)}{\Big(1 - \beta + \beta e^{\lambda r}\Big)^3}. \end{aligned}$$

The result follows by noting that the above partial derivatives are strictly negative for any $\lambda > 0$ and $\beta \in (0, 1]$. ∎

Proof of Part (b): To demonstrate that $v_{\lambda,\beta}$ is non-convex we simply exhibit a (λ_1, β_1) and a (λ_2, β_2) along with a $\theta \in [0, 1]$ such that $\theta v_{\lambda_1,\beta_1} + (1-\theta) v_{\lambda_2,\beta_2} < v_{\bar{\lambda},\bar{\beta}}$ (where $(\bar{\lambda}, \bar{\beta}) = \theta(\lambda_1, \beta_1) + (1-\theta)(\lambda_2, \beta_2)$), thus defying the condition necessary for convexity [26]. For instance, let $\lambda_1 = 0.1$, $\lambda_2 = 3.5$ and $\beta_1 = \beta_2 = 0.01$. Then, for $\theta = 0.5$ (with $r = 1$[6]), we obtain $v_{\lambda_1,\beta_1} = 0.99$, $v_{\lambda_2,\beta_2} = 0.57$ and $v_{\bar{\lambda},\bar{\beta}} = 0.90$, while $\theta v_{\lambda_1,\beta_1} + (1-\theta) v_{\lambda_2,\beta_2} = 0.78 < v_{\bar{\lambda},\bar{\beta}}$.

Similarly, to show non-concavity, consider $\lambda_1 = 4$, $\lambda_2 = 6$ and $\beta_1 = \beta_2 = 0.01$. Then, again for $\theta = 0.5$ (with $r = 1$), we obtain $v_{\lambda_1,\beta_1} = 0.42$, $v_{\lambda_2,\beta_2} = 0.04$, and $v_{\bar{\lambda},\bar{\beta}} = 0.16$ while $\theta v_{\lambda_1,\beta_1} + (1-\theta) v_{\lambda_2,\beta_2} = 0.23 > v_{\bar{\lambda},\bar{\beta}}$, thus defying the condition necessary for concavity [26].

See Fig. 9(a) for an illustration of the non-convexity and non-concavity behavior of the vacancy function $v_{\lambda,\beta}$ around the above considered values. ∎

Proof of Part (c): In order to prove quasi-convexity we will show that the sub-level set $\mathcal{C}_\alpha = \{(\lambda, \beta) : v_{\lambda,\beta} \le \alpha\}$, where $\alpha \in (0, 1]$, is convex[7]. For this, we first express the level set $\{(\lambda, \beta) : v_{\lambda,\beta} = \alpha\}$ as the graph $\{(\lambda(\beta), \beta) : v_{\lambda(\beta),\beta} = \alpha\}$. Solving for λ from the equation $v_{\lambda,\beta} = \alpha$ we have

$$\lambda(\beta) = \frac{1}{r} \ln\left(1 + \frac{\tilde{\alpha}}{\beta}\right)$$

where $\tilde{\alpha} = \frac{1-\sqrt{\alpha}}{\sqrt{\alpha}} > 0$. Since the second-derivative

$$\lambda''(\beta) = \frac{\tilde{\alpha}(\tilde{\alpha} + 2\beta)}{r\beta^2(\tilde{\alpha} + \beta)^2} > 0 \quad \text{for all } \beta \in (0, 1]$$

[6]For simplicity, we fix $r = 1$. Note that, similar instances can be exhibited for other values of r as well.

[7]For $\alpha > 1$, $C_\alpha = \{(\lambda, \beta) : \lambda > 0, \beta \in (0, 1]\}$ is readily convex. Hence, we only consider the case $\alpha \in (0, 1]$.

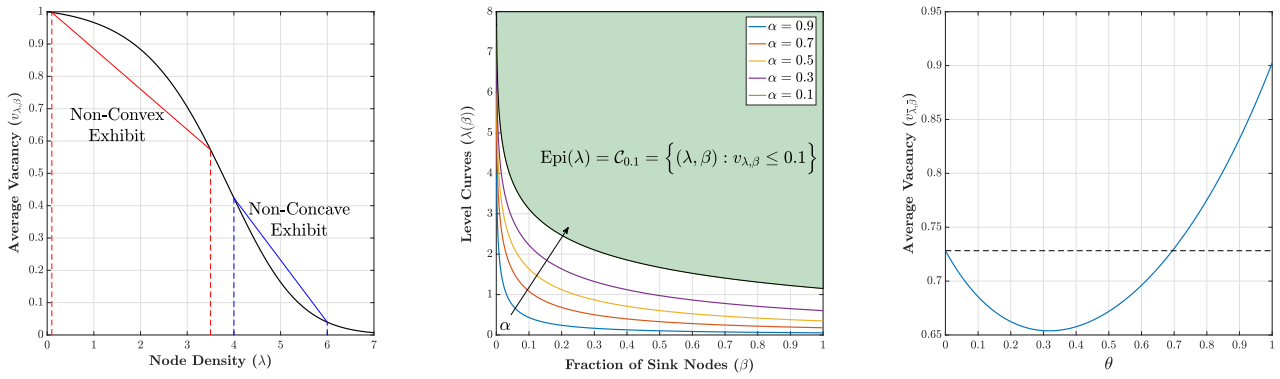

(a) (b) (c)

Fig. 9. Illustrations supporting the details in the proof of Lemma 3. (a) Non-convex and non-concave behavior of the average vacancy function $v_{\lambda,\beta}$; (b) Level curves $\lambda(\beta)$ of the function $v_{\lambda,\beta}$. The shaded region represents the epigraph of the level curve corresponding to $\alpha = 0.1$, which is shown to be equal to the sub-level set $\mathcal{C}_{0.1}$. (c) Illustration depicting the non-concave nature of the vacancy function $v_{\lambda,\beta}$.

it follows that $\lambda(\beta)$ is strictly convex (see Fig. 9(b)). Hence, the epigraph of the function λ, given by

$$\text{Epi}(\lambda) = \{(t,\beta) : \beta \in (0,1], \lambda(\beta) \le t\}$$

is convex [26]. Finally, since $v_{\lambda,\beta}$ is decreasing in λ (recall Part (a)), it follows that $C_\alpha = \text{Epi}(\lambda)$, thus completing the proof of quasi-convexity.

To show that $v_{\lambda,\beta}$ is not quasi-concave, consider the following points: $(\lambda_1,\beta_1) = (0.1, 0.5)$ and $(\lambda_2,\beta_2) = (1, 0.1)$. Then, for $\theta = 0.3$ (with $r = 1$) we obtain $v_{\lambda_1,\beta_1} = 0.90$ and $v_{\lambda_2,\beta_2} = 0.73$ while $v_{\bar{\lambda},\bar{\beta}} = 0.65 < \min\{v_{\lambda_1,\beta_1}, v_{\lambda_2,\beta_2}\}$, thus defying the condition necessary for quasi-concavity. The above non-quasi-concave behavior is depicted in Fig 9(c). ■

C. Proof of Theorem 2

Proof: Let $\{Y_k : k \ge 1\}$ be the locations of the sink nodes in the independent-disk model. Thus, the sink node locations are coupled in both models. We will use $\widehat{U}_k$ and $\widehat{V}_k$, respectively, to denote the lengths of the coverage disk towards the right and left of Y_k in the independent-disk model. Thus, $\widehat{\mathcal{W}}_k := [Y_k - \widehat{V}_k, Y_k + \widehat{U}_k]$ is the coverage disk around Y_k in the independent-disk model. These quantities are iteratively obtained as follows.

Define $k_1 = 1$. Let $\widehat{U}_{k_1} = U_{k_1}$ and $\widehat{V}_{k_1} = V_{k_1}$. Thus, we have $\widehat{\mathcal{W}}_{k_1} = \mathcal{W}_{k_1}$. Define $T_1 := Y_{k_1} + \widehat{U}_{k_1}$. Note that, given the sequence $\{Y_k\}$, T_1 is a *stopping time* for Λ, i.e., $\{T_1 \le t\}$ depends only on the process $\{\Lambda([0,\tau]) : \tau \le t\}$. Thus, the process, $\Lambda' := \{\Lambda([T_1, T_1+t]) : t \ge 0\}$ is a one-sided Poisson process of rate $(1-\beta)\lambda$, independent of $(\widehat{V}_{k_1}, \widehat{U}_{k_1})$.

Let Ω_1 denote a Poisson process on $\Re$ of rate $(1-\beta)\lambda$, that is independent of Λ. Construct a new point process, Λ_1, by concatenating the points of Ω_1 and Λ as follows:

$$\Lambda_1([a,b]) = \begin{cases} \Omega_1([a,b]) & \text{if } b \le T_1 \\ \Lambda([a,b]) & \text{if } a \ge T_1 \\ \Omega_1([a,T_1]) + \Lambda((T_1,b]) & \text{otherwise.} \end{cases} \quad (50)$$

It follows that Λ_1 is also a Poisson process of rate $(1-\beta)\lambda$ [27, Section 3.3]. Further, Λ_1 is independent of $(\widehat{V}_{k_1}, \widehat{U}_{k_1})$ (since Λ' and Ω_1 are independent of $(\widehat{V}_{k_1}, \widehat{U}_{k_1})$).

Now, define $k_2 = \min\{k > k_1 : Y_k > T_1 - r\}$. Using the points of Λ_1 as the location of the relay nodes, obtain the coverage disk, $\widehat{\mathcal{W}}_{k_2} := [Y_{k_2} - \widehat{V}_{k_2}, Y_2 + \widehat{U}_{k_2}]$, where $\widehat{V}_{k_2}$ and $\widehat{U}_{k_2}$ denote the disk's length towards the left and right of Y_{k_2}, respectively. $(\widehat{V}_{k_2}, \widehat{U}_{k_2})$ is independent and identically distributed as $(\widehat{V}_{k_1}, \widehat{U}_{k_1})$, since the process Λ_1 is independent of the latter. In the following we will show that

$$\bigcup_{k=1}^{k_2} \mathcal{W}_k \subseteq \widehat{\mathcal{W}}_{k_1} \cup \widehat{\mathcal{W}}_{k_2}. \quad (51)$$

First, recalling the definition of k_2, note that we have $Y_{k_1} \le Y_k \le T_1 - r$, for all $k_1 < k < k_2$. Thus, Y_k is surrounded by the same set of relay nodes that determine U_{k_1}. Hence, U_k satisfies, $Y_k + U_k = Y_{k_1} + U_{k_1}$. On the other hand, there are two cases possible for V_k: (i) $Y_k - V_k > Y_{k_1} - V_{k_1}$, if the connectivity between the relay nodes on either side of Y_{k_1} is affected after removing Y_{k_1}; otherwise (ii) $Y_k - V_k = Y_{k_1} - V_{k_1}$. In general, V_k satisfies, $Y_k - V_k \ge Y_{k_1} - V_{k_1}$. Thus, we have

$$\mathcal{W}_k \subseteq \mathcal{W}_{k_1} = \widehat{\mathcal{W}}_{k_1}, \text{ for all } k_1 < k < k_2. \quad (52)$$

Next, we proceed to characterize the coverage disk around Y_{k_2}. We need to consider two cases: (i) $Y_{k_2} \in (T_1 - r, T_1)$ and (ii) $Y_{k_2} \ge T_1$.

Case-(i): If $U_{k_2} = r$ (implying $\Lambda([Y_{k_2}, Y_{k_2} + r]) = 0$) then $\widehat{U}_{k_2} \ge U_{k_2}$. This is because, if $\Omega_1([Y_{k_2}, T_1]) > 0$ then it is possible that a point of Ω_1 in $[Y_{k_2}, T_1]$ is connected to a point of Λ in $[Y_{k_2} + r, \infty)$, thus extending the right coverage disk of Y_{k_2} in the independent-disk model. On the other hand, if $U_{k_2} > r$ then $\widehat{U}_{k_2} = U_{k_2}$, since in both models these quantities are determined by the points of Λ in $[T_1, \infty)$. Thus, in general, we have

$$[Y_{k_2}, Y_{k_2} + U_{k_2}] \subseteq [Y_{k_2}, Y_{k_2} + \widehat{U}_{k_2}] \subseteq \widehat{\mathcal{W}}_{k_2}. \quad (53)$$

Recalling the argument used for V_k ($k_1 < k < k_2$), we have, $Y_{k_2} - V_{k_2} \ge Y_{k_1} - V_{k_1}$, so that

$$[Y_{k_2} - V_{k_2}, Y_{k_2}] \subseteq \mathcal{W}_{k_1} = \widehat{\mathcal{W}}_{k_1}. \quad (54)$$

Combining (53) and (54) we see that, $\mathcal{W}_{k_2} \subseteq \widehat{\mathcal{W}}_{k_1} \cup \widehat{\mathcal{W}}_{k_2}$. Using the above along with (52), we obtain (51).

$$f_{G_\ell}^{(\alpha)}(x) = \begin{cases} f_{G_{\ell-1}}(x) - \sum_{k=2,4,\cdots}^{\ell-2} \theta_\alpha^{\frac{(\ell-2)-k}{2}} \Big(\mu r f_{G_k}(x) - f_{G_{k-1}}(x)\Big) e^{-\mu r} - \theta_\alpha^{\left(\frac{\ell}{2}-1\right)} \mu e^{-\mu r} & \text{if } \ell \text{ is even} \\ f_{G_{\ell-1}}(x) - \sum_{k=3,5,\cdots}^{\ell-2} \theta_\alpha^{\left\lfloor\frac{(\ell-2)-k}{2}\right\rfloor} \Big(\mu r f_{G_k}(x) - f_{G_{k-1}}(x)\Big) e^{-\mu r} - \theta_\alpha^{\left\lfloor\frac{\ell}{2}-1\right\rfloor} \mu x e^{-\mu r} f_{G_1}(x) & \text{if } \ell \text{ is odd} \end{cases} \quad (57)$$

Case-(ii): Recall that this case corresponds to $Y_{k_2} \geq T_1$. Since $\Lambda_1 = \Lambda$ in $[T_1, \infty)$, U_{k_2} and $\widehat{U}_{k_2}$ are obtained using the same Poisson points of relay nodes. Hence, we readily have $\widehat{U}_{k_2} = U_{k_2}$. To obtain $\widehat{V}_{k_2}$, note that V_{k_2} satisfies $Y_{k_2} - V_{k_2} > T_1 - r$ (since $\Lambda([T_1 - r, T_1]) = 0$). If $Y_{k_2} - V_{k_2} > T_1$ then $\widehat{V}_{k_2} = V_{k_2}$ since $\Lambda_1 = \Lambda$ on $(T_1, Y_{k_2}]$. In contrast, if $Y_{k_2} - V_{k_2} \in (T_1 - r, T_1]$ then $\widehat{V}_{k_2} \geq V_{k_2}$ since it is possible that a point of Ω_1 in $(T_1 - r, T_1]$ is connected to a point of Λ in (T_1, ∞) so that the left coverage disk of Y_{k_2} gets extended in the independent-disk model. Thus, we have

$$\mathcal{W}_{k_2} \subseteq \widehat{\mathcal{W}}_{k_2}. \quad (55)$$

Combining (52) and (55) we see that (51) is satisfied for case-(ii) as well.

We complete the proof through an induction argument. Suppose for some $n \geq 2$ we have inductively obtained i.i.d. coverage disks, $\widehat{\mathcal{W}}_{k_m} = [Y_{k_m} - \widehat{V}_{k_m}, Y_{k_m} + \widehat{U}_{k_m}]$, for $m = 1, 2, \cdots, n$, satisfying,

$$\bigcup_{k=1}^{k_n} \mathcal{W}_k \subseteq \bigcup_{m=1}^{n} \widehat{\mathcal{W}}_{k_m}. \quad (56)$$

Define $T_k = Y_{k_n} + \widehat{U}_{k_n}$ and $k_{n+1} = \min\{k > k_n : Y_k > T_k - r\}$. Let Ω_k be a Poisson process of rate $(1-\beta)\lambda$, independent of Λ and $\Omega_m, m = 1, 2, \cdots, k-1$. Analogous to the construction of Λ_1 in (50), obtain the Poisson process Λ_k by concatenating the processes Ω_k and Λ at T_k. Since T_k is a stopping time for Λ, it follows that Λ_k is independent of $\widehat{\mathcal{W}}_{k_m}, m = 1, 2 \cdots, n$. Using the points of Λ_k as the location of the relay nodes, we can obtain i.i.d. coverage disk, $\widehat{\mathcal{W}}_{k_{n+1}} = [Y_{k_{n+1}} - \widehat{V}_{k_{n+1}}, Y_{k_{n+1}} + \widehat{U}_{k_{n+1}}]$, around $Y_{k_{n+1}}$.

Now, for all k such that $k_n < k < k_{n+1}$ we have $Y_{k_n} \leq Y_k \leq T_k - r$. Hence, as in $n = 2$ case, U_k and V_k, respectively, satisfies $Y_k + U_k = Y_{k_n} + U_{k_n}$ and $Y_k - V_k \geq Y_{k_n} - V_{k_n}$, thus yielding,

$$\mathcal{W}_k \subseteq \mathcal{W}_{k_n}, \text{ for all } k_n < k < k_{n+1}. \quad (58)$$

Again, using the arguments analogous to the $n = 2$ case, we can show that $\mathcal{W}_{k_{n+1}}$ satisfies,

$$\mathcal{W}_{k_{n+1}} \subseteq \begin{cases} \bigcup_{m=1}^{n+1} \widehat{\mathcal{W}}_{k_m} & \text{if } Y_{k_{n+1}} \in (T_k - r, T_k) \\ \widehat{\mathcal{W}}_{k_{n+1}} & \text{if } Y_{k_{n+1}} \geq T_k. \end{cases} \quad (59)$$

Using (56), (58) and (59) we finally obtain,

$$\bigcup_{k=1}^{k_{n+1}} \mathcal{W}_k \subseteq \bigcup_{m=1}^{n+1} \widehat{\mathcal{W}}_{k_m}$$

thus completing the induction argument. ∎

D. Proof of Theorem 3

Proof: We will first show that the result holds for $\ell = 2$. In order to compute $\overline{G}_2$, we require the conditional density of G_2 given G_1. In general, for $\ell \geq 2$, using $\mathbb{P}_{h,y}$ to denote the probability measure conditioned on $\{G_{\ell-1} = y\}$ (where $y \in [0, r]$), we have

$$\mathbb{P}_{h,y}(G_\ell \leq x) = \begin{cases} e^{-\mu y} & \text{if } x \leq r - y \\ e^{-\mu(r-x)} & \text{if } x \in [r-y, r] \end{cases}$$

Thus, the conditional density of G_ℓ given $G_{\ell-1}$, denoted $f_{G_\ell|G_{\ell-1}}(\cdot|\cdot)$, can be written as

$$f_{G_\ell|G_{\ell-1}}(x|y) = \begin{cases} \mu e^{-\mu(r-x)} & \text{for } x \in [r-y, r] \\ 0 & \text{otherwise.} \end{cases} \quad (60)$$

Note that the conditional density does not depend on the index ℓ. Also, from (31) observe that $f_{G_\ell|G_{\ell-1}}(x|y) = f_{G_1}(x)$. These observations will be useful in our subsequent development.

Now, using the conditional density $f_{G_\ell|G_{\ell-1}}$, the density function of G_ℓ can be computed as follows:

$$\begin{aligned} f_{G_\ell}(x) &= \int_0^r f_{G_{\ell-1}}(y) f_{G_\ell|G_{\ell-1}}(x|y) dy \\ &= \int_{r-x}^r f_{G_{\ell-1}}(y) f_{G_1}(x) dy. \end{aligned} \quad (61)$$

Simplifying the above expression for $h = 2$ we obtain,

$$f_{G_2}(x) = f_{G_1}(x) - \mu e^{-\mu r}. \quad (62)$$

Thus, $\overline{G}_2 = \mathbb{E}[G_2]$ is given by

$$\overline{G}_2 = \overline{G}_1 - \frac{\mu r^2}{2} e^{-\mu r}. \quad (63)$$

Similarly, for $\ell = 3$ we have

$$\begin{aligned} f_{G_3}(x) &= \int_0^r f_{G_2}(y) f_{G_2|G_1}(x|y) dy \\ &= \int_{r-x}^r \Big(f_{G_1}(y) - \mu e^{-\mu r}\Big) f_{G_1}(x) dy \\ &= \int_{r-x}^r f_{G_1}(y) f_{G_1}(x) dy - \int_{r-x}^r \mu e^{-\mu r} f_{G_1}(x) dy \\ &= f_{G_2}(x) - \mu x e^{-\mu r} f_{G_1}(x) \end{aligned} \quad (64)$$

where the last equality is obtained using (61) with $\ell = 2$. The expectation of G_3 is thus given by

$$\overline{G}_3 = \overline{G}_2 - \mu \overline{\overline{G}}_1 e^{-\mu r}. \quad (65)$$

Comparing (63) and (65) with the expression for $\overline{G}_2^{(\alpha)}$ and $\overline{G}_3^{(\alpha)}$ in (37) and (38), respectively, we see that (39) and (40)

trivially holds for $\ell = 2, 3$. We will complete the proof by induction. Suppose for some $\ell \geq 2$ we have, for all $x \in [0, r]$,

$$f^{(r)}_{G_\ell}(x) \leq f_{G_\ell}(x) \leq f^{(0)}_{G_\ell}(x) \quad (66)$$

$$f^{(r)}_{G_\ell}(x) \leq f^{(\alpha)}_{G_\ell}(x) \leq f^{(0)}_{G_\ell}(x) \quad (67)$$

where $f^{(\alpha)}_{G_\ell}(x)$ is defined as in (57).

Expressions (66) and (67) are the induction hypothesis. Note that, since

$$\int_0^r x f^{(\alpha)}_{G_\ell}(x)dx \quad = \quad \overline{G}^{(\alpha)}_\ell$$

(66) and (67) implies the results in (39) and (40), respectively (thus, we are assuming a stronger induction hypothesis). Also, from (62) and (64) observe that (66) and (67) already holds for $\ell = 2, 3$.

First, let us consider the case where ℓ is even. Then, since $f_{G_\ell|G_{\ell-1}}(x|y) = f_{G_1}(x)$ (recall the discussion following (60)) and $\int_{r-x}^r f_{G_k}(y) f_{G_1}(x)dy = f_{G_{k+1}}$ (see (61)), we obtain

$$\int_0^r f^{(\alpha)}_{G_\ell}(y) f_{G_1}(x)dy \quad = \quad f^{(\alpha)}_{G_{\ell+1}}(x).$$

The above expression, along with the induction hypothesis, can be used to show that the inequalities in (66) and (67) hold for $\ell + 1$.

Next, suppose ℓ is odd, then $\int_{r-x}^r f^{(\alpha)}_{G_\ell}(y) f_{G_1}(x)dy$ will involve an integral term of the form

$$g^{(\alpha)}(x) \quad := \quad c_\alpha \int_{r-x}^r \mu y e^{-\mu r} f_{G_1}(y) f_{G_1}(x)dy$$

where for simplicity we have let $c_\alpha := \theta_\alpha^{\lfloor \frac{\ell}{2} - 1 \rfloor}$. The above expression can be simplified to yield

$$g^{(\alpha)}(x) \quad = \quad c_\alpha \Big(\mu r f_{G_2}(x) - f_{G_1}(x) \Big) e^{-\mu r} + c_\alpha \theta_x \mu e^{-\mu r}.$$

For $\alpha = 0$ and $\alpha = r$, respectively, replacing θ_x in the RHS of the above expression by θ_α, we obtain

$$\begin{aligned} g^{(r)}(x) &\leq c_r \Big(\mu r f_{G_2}(x) - f_{G_1}(x) \Big) e^{-\mu r} + c_r \theta_r \mu e^{-\mu r} \\ g^{(0)}(x) &\geq c_0 \Big(\mu r f_{G_2}(x) - f_{G_1}(x) \Big) e^{-\mu r} + c_0 \theta_0 \mu e^{-\mu r}. \end{aligned}$$

Using the above inequalities, along with (66), we obtain

$$\begin{aligned} f^{(r)}_{G_{\ell+1}}(x) &\leq \int_{r-x}^r f^{(r)}_{G_\ell}(y) f_{G_1}(x)dy \\ &\leq \int_{r-x}^r f_{G_\ell}(y) f_{G_1}(x)dy \\ &= f_{G_{\ell+1}}(x) \\ &\leq \int_{r-x}^r f^{(0)}_{G_\ell}(y) f_{G_1}(x)dy \\ &\leq f^{(0)}_{G_{\ell+1}}(x). \end{aligned}$$

Finally, since $\theta_0 \leq \theta_\alpha \leq \theta_r$, from (67) it follows that $f^{(r)}_{G_{\ell+1}}(x) \leq f^{(\alpha)}_{G_{\ell+1}}(x) \leq f^{(0)}_{G_{\ell+1}}(x)$. ∎

E. Properties of the Cost Function

Recall the expression for the cost function:

$$\begin{aligned} c_{\lambda,\beta} &= \lambda\beta c_S + \lambda(1-\beta)c_R \\ &= \lambda\beta(c_S - c_R) + \lambda c_R \end{aligned} \quad (68)$$

where c_S and c_R are the cost of the sink and relay nodes, respectively. Note that, we assume $c_S > c_R$. Although convexity and quasi-convexity results for the form of expression in (68) is well known [26], we formally report these results here for completeness.

Lemma 6: (a) $c_{\lambda,\beta}$ is neither convex nor concave.

(b) $c_{\lambda,\beta}$ is not quasi-convex but is quasi-concave.

Proof of Part (a): The Hessian matrix of the cost function in (68) can be written as

$$\nabla^2 c_{\lambda,\beta} = \begin{bmatrix} 0 & (c_S - c_R) \\ (c_S - c_R) & 0 \end{bmatrix}.$$

Now the result follows since the above matrix is neither positive semidefinite nor negative semidefinite. ∎

Proof of Part (b): To show that $c_{\lambda,\beta}$ is not quasi-convex, consider the following points: $(\lambda_1, \beta_1) = (0.1, 1)$ and $(\lambda_2, \beta_2) = (1, 0.1)$. Then, with $c_S = 4$ and $c_R = 1$, we have $v_{\lambda_1,\beta_1} = 0.4$ and $v_{\lambda_2,\beta_2} = 1.3$, while for $\theta = 0.3$ we obtain $v_{\bar{\lambda},\bar{\beta}} = 1.54 > \max\{v_{\lambda_1,\beta_1}, v_{\lambda_2,\beta_2}\}$ where $(\bar{\lambda}, \bar{\beta}) = \theta(\lambda_1, \beta_1) + (1-\theta)(\lambda_2, \beta_2)$. The above inequality defies the condition that is necessary for quasi-convexity.

To prove quasi-concavity, we invoke the *first-order condition* [26] which states that $c_{\lambda,\beta}$ is quasi-concave iff

$$c_{\lambda_2,\beta_2} \geq c_{\lambda_1,\beta_1} \implies \langle \nabla c_{\lambda_1,\beta_1}, (\lambda_2, \beta_2) - (\lambda_1, \beta_1) \rangle \geq 0 \quad (69)$$

where $\nabla c_{\lambda_1,\beta_1}$ denotes the gradient of $c_{\lambda,\beta}$ evaluated at (λ_1, β_1) while $\langle \cdot, \cdot \rangle$ represents inner product. The second inequality in (69) can be simplified to obtain:

$$\Delta_c \beta_1 (\lambda_2 - \lambda_1) \geq \Delta_c \lambda_1 (\beta_1 - \beta_2) + c_R(\lambda_1 - \lambda_2) \quad (70)$$

where, $\Delta_c = (c_S - c_R)$. Similarly, subtracting $\delta_c \lambda_1 \beta_2$ from both sides of the first inequality in (69) and simplifying yields

$$\Delta_c \beta_2 (\lambda_2 - \lambda_1) \geq \Delta_c \lambda_1 (\beta_1 - \beta_2) + c_R(\lambda_1 - \lambda_2). \quad (71)$$

Three cases are possible depending on the relative values of β_1 and β_2. (*Case-1*) If $\beta_1 = \beta_2$ then (71) trivially implies (70). (*Case-2*) Suppose $\beta_1 > \beta_2$ then invariably it should be that $\lambda_1 < \lambda_2$ (otherwise the hypothesis (71) will be violated) so that the LHS of (71) is positive; β_2 in the LHS can hence be replaced by $\beta_1 > \beta_2$, yielding (70). (*Case-3*) Finally, suppose $\beta_1 < \beta_2$ then the following two sub-cases are possible:

- If $\lambda_1 \leq \lambda_2$ then the LHS of (71) is non-negative while the RHS is strictly negative. Thus, β_2 in the LHS of (71) can be replaced by β_1 to yield (70).
- On the other hand, if $\lambda_1 > \lambda_2$ then both the LHS and the RHS of (71) are negative. Thus, β_2 in the LHS of (71) can again be replaced by $\beta_1 < \beta_2$ to obtain (70).

We have thus shown that (69) holds. The first-order condition then implies that $c_{\lambda,\beta}$ is quasi-concave. ∎